EurJOC European Journal of Organic Chemistry

FULL PAPER

DOI: 10.1002/ejoc.201200688

Arylamine-Modified Thiazoles as Donor–Acceptor Dyes: Quantum Chemical Evaluation of the Charge-Transfer Process and Testing as Ligands in Ruthenium(II) Complexes

Roberto Menzel,[a][‡] Stephan Kupfer,[b,c][‡] Ralf Mede,[a] Dieter Weiß,[a] Helmar Görls,[d] Leticia González,*[c] and Rainer Beckert*[a]

Keywords: N,S-Heterocycles / Heterocycles / Chromophores / Dyes / Charge transfer / Density functional calculations / Ruthenium complexes

A series of new 4-hydroxy-1,3-thiazole-based chromophores bearing different arylamine components (triarylamines, carbazole, and phenothiazine) as electron donors and azaheterocycle components (pyridine, pyrazine and pyrimidine) as electron-acceptor moieties have been synthesized. Elaborate quantum chemical calculations were carried out with two selected compounds to identify the natures of the HOMO/LUMO transition and of the intramolecular charge-transfer state. The electrochemical properties were investigated: the dyes show reversible first oxidation and reduction peaks, with the former strongly dominated by the type of arylamine. The donor moieties were synthesized under Buchwald–Hartwig conditions. Several of the presented X-ray structures provide deeper insight into the geometries of the ligands. The bidentate nature of the chromophores makes them suitable as ligands in transition metal complexes. The corresponding ruthenium(II) polypyridine complexes – $Ru(dmbpy)_2(\mathbf{L})(PF_6)_2$ (dmbpy = 4,4′-dimethyl-2,2′-bipyridine) – were successfully synthesized for seven of the ligands. The MLCT bands in these complexes are significantly broadened, resulting in improved light-harvesting efficiencies.

Introduction

The classical heterocyclic 4-hydroxy-1,3-thiazole core was described by R. Dodson and H. Turner in 1951.[1] Since then, several compounds have been synthesized[2] but only a few data relating to applications of these compounds exist. Some of the derivatives have been tested as drugs (e.g., as cyclooxygenase, 5-lipoxygenase, and cyclin-dependent kinase 5 inhibitors).[3]

Our group revived the 4-hydroxy-1,3-thiazole unit as a chromophore and fluorophore, due to its similarities to the naturally occurring luciferin and its remarkable spectroscopic characteristics. Several applications of its derivatives have been developed since then. Thanks to their easy functionalization and tunable optical properties they have been successfully incorporated as blue-emitting species in a polymer backbone,[4] as a FRET energy donor in a terpolymer together with a Ru^{II} complex as the acceptor unit,[5] and as chromophores in donor-π-acceptor (D-π-A) dyes in dye-sensitized solar cells (DSSCs).[6] In addition, they were very recently reported to be fast and specific systems for fluoride ion detection[7] and have been employed as light-harvesting ligands in Ru^{II} polypyridyl complexes.[8]

The last of these in particular is of significant interest, due to the potential application of Ru^{II} dyes as sensitizers in DSSCs, which usually lack chromophores to harvest sunlight efficiently. Furthermore, ruthenium(II) complexes, especially Ru^{II} polypyridine complexes, have attracted considerable interest due to their outstanding properties, such as good chemical stability, reversible redox behavior, and long-lived excited states with distinct reactivities and unique, tunable emission characteristics.[9] This has opened the doorway to numerous applications.[10] Nonetheless, the investigation of new complexes is still an evolving field and is one part of this contribution.

Additionally, arylamines have also been the focus of intense research, due to potential applications in various functional materials. They have been used as materials that show photoconductive and nonlinear optical (NLO) properties,[11] and were employed for that purpose as chromo-

[a] Friedrich Schiller University Jena, Institute of Organic and Macromolecular Chemistry,
Humboldtstraße 10, 07743 Jena, Germany
Fax: +49-3641-948212
E-mail: c6bera@uni-jena.de
Homepage: http://www.agbeckert.uni-jena.de/
[b] Friedrich Schiller University Jena, Institute of Physical Chemistry,
Helmholtzweg 4, 07743 Jena, Germany
[c] University of Vienna, Institute of Theoretical Chemistry,
Waehringer Str. 17, 1090 Vienna, Austria
Homepage: http://theochem.univie.ac.at/
[d] Friedrich Schiller University Jena, Institute of Inorganic and Analytical Chemistry,
Humboldtstraße 8, 07743 Jena, Germany
[‡] Both authors contributed equally to this article
Supporting information for this article is available on the WWW under http://dx.doi.org/10.1002/ejoc.201200688.

phores in ultrafast electro-optic (EO) applications.[12] Furthermore, they can act as photoconductors and hole-transporting materials in organic light-emitting diodes (OLEDS),[13] and are promising cores both in bulk heterojunction (BHJ) solar cells[14] and in Grätzel-type DSSCs.[15]

The synthesis and characterization of different dyes based on the 4-methoxy-1,3-thiazole core as a chromophore with an arylamine donor in the 5-position (i.e., with a phenyl-, *p*-anisole-, *p*-tolyl-, or phenothiazine-based arylamine) and a pyridine, pyrimidine, or pyrazine moiety in the 2-position as acceptor is presented. Two of the dyes were further investigated by quantum chemical methods in order to assign their longest-wavelength absorptions either to a twisted (TICT) or to a planar (PICT) intramolecular charge-transfer process. The successful synthesis of seven heteroleptic Ru^{II} complexes was achieved by use of the activated precursor *cis*-$Ru(dmbpy)_2(acetone)_2(PF_6)_2$.[16] The complexes were synthesized in order to test the abilities and characteristics of these dyes as ligands, which is considered a first step to establishing this class of chromophores as electron-donating and light-harvesting ligands in Ru^{II} complexes utilized as sensitizers in DCCSs.[17] All compounds were investigated with regard to their electronic and electrochemical properties. Furthermore, the emission behavior of the dyes was characterized in terms of lifetime and quantum efficiency measurements.

Results and Discussion

Synthesis

The synthesis of the dyes/ligands is depicted in Scheme 1. The new 4-hydroxy-1,3-thiazoles **1a**–**1c** were prepared by Hantzsch thiazole cyclizations between the thioamides of the corresponding azaheterocycles and ethyl 2-bromo-2-(4-nitrophenyl)acetate, which can in turn easily be prepared from the commercially available 2-(4-nitrophenyl)acetic acid by a standard protocol.[18] Compound **1d** was prepared similarly, from ethyl 2-bromo-2-(4-bromophenyl)acetate and pyridine-2-carbothioamide, as described in the literature.[19] Alkylation of the "phenolic" 4-hydroxy group was achieved in a manner similar to the Williamson ether synthesis, by treatment of the deprotonated thiazole with methyl iodide in DMSO. The reduction of the nitro group in **2a**–**2c** was accomplished with freshly prepared Raney nickel and hydrazine as the hydrogen source in EtOH in excellent yields (>95%).

The bottleneck for the synthesis of the arylamines was the Buchwald–Hartwig cross-coupling reaction, involving a double *N*-arylation. Although thoroughly described in the literature, the reaction depends strongly on the natures of the catalysts and ligands and on the conditions used.[20] Several attempts with, for example, triphenylphosphane or 1,1′-bis(diphenylphosphanyl)ferrocene as ligand together with NaH or KO*t*Bu as base have failed completely. Therefore, the electron-rich ligand tri-*tert*-butylphosphane [P(*t*Bu)$_3$], which had already been successfully applied in the synthesis of different carbazole derivatives,[21] was chosen as a promising candidate. For the coupling reaction, bis(dibenzylideneacetone)palladium(0) [Pd(dba)$_2$] was used as the precatalyst, KO*t*Bu as the base to deprotonate the amine in the catalytic cycle, and toluene as solvent. Fortunately, the desired products were obtained with use of P(*t*Bu)$_3$ in good yields (76–90%). In addition, the two-step nature of the reaction was demonstrated. As representative examples, for **A1** and **B1** the monosubstituted products **A1m** (69%) and **B1m** (88%) were obtained. This opens the door for the construction of unsymmetrically substituted triarylamines useful for photonic applications.[22] Unlike the double *N*-arylation of the amines **3a**–**3c**, the Buchwald–Hartwig reaction starting with **2d**, in which the aryl halide is connected to the thiazole, was not successful by the described method: with the commonly used diphenylamine as the amine component no conversion to the substituted product was observed under various conditions. The biarylphosphane ligand 2-(dicyclohexylphosphanyl)-2′,6′-dimethoxy-1,1′-biphenyl (SPHOS) was therefore chosen as a promising ligand.[20b,23] SPHOS has already been successfully applied in the amination of chloro-terpyridine and is widely used in the Suzuki–Miyaura reaction.[24] Finally, the coupling reaction with employment of SPHOS yielded the arylamines **D1**–**D3** (69 to 88%).

The synthesis of the heteroleptic Ru^{II} complexes is also depicted in Scheme 1. The standard procedure – heating of precursor *cis*-$(dmbpy)_2RuCl_2$ (1 equiv.) in EtOH with the appropriate ligand (1 equiv.) for 24 h under reflux conditions and precipitating the product with NH_4PF_6 – yielded an inseparable mixture of products, so the precursor was activated with $AgPF_6$ prior to the complexation reaction with the ligand. The synthesized complexes can easily be purified by size exclusion chromatography either with Bio-Beads® S-X1 with DCM or with Sephadex® LH-20 with acetone as solvent if they are only sparingly soluble in DCM. After precipitation of the products with diethyl ether, they were obtained as deep red solids in moderate to good yields (75–93%). Although several attempts were made, it was not possible to obtain pure samples of all possible complexes. No homogeneous products were obtained in the cases of compounds **B1** and **B2**. Most likely unfavorable complexation at the second pyrazine nitrogen atom led to a mixture of differently substituted complexes. The complexation was also unsuccessful in the case of ligand **A3**.

X-ray Structures

X-ray structures of the molecules **A1**, **B1**, **C1**, and **D2** were obtained from crystals grown directly in NMR tubes by slow evaporation of $CHCl_3$/EtOH solvent mixtures. The structures are depicted in Figure 1 and data are listed in Table 1 (additional refinement data are reported in Scheme S1 in the Supporting Information). Each dye shows a more or less planar geometry along the acceptor 1,3-thiazole unit, with the nitrogen atoms arranged in a *transoid* conformation due to N–H hydrogen-bonding interactions between N1 of the 1,3-thiazole and the hydrogen of the ap-

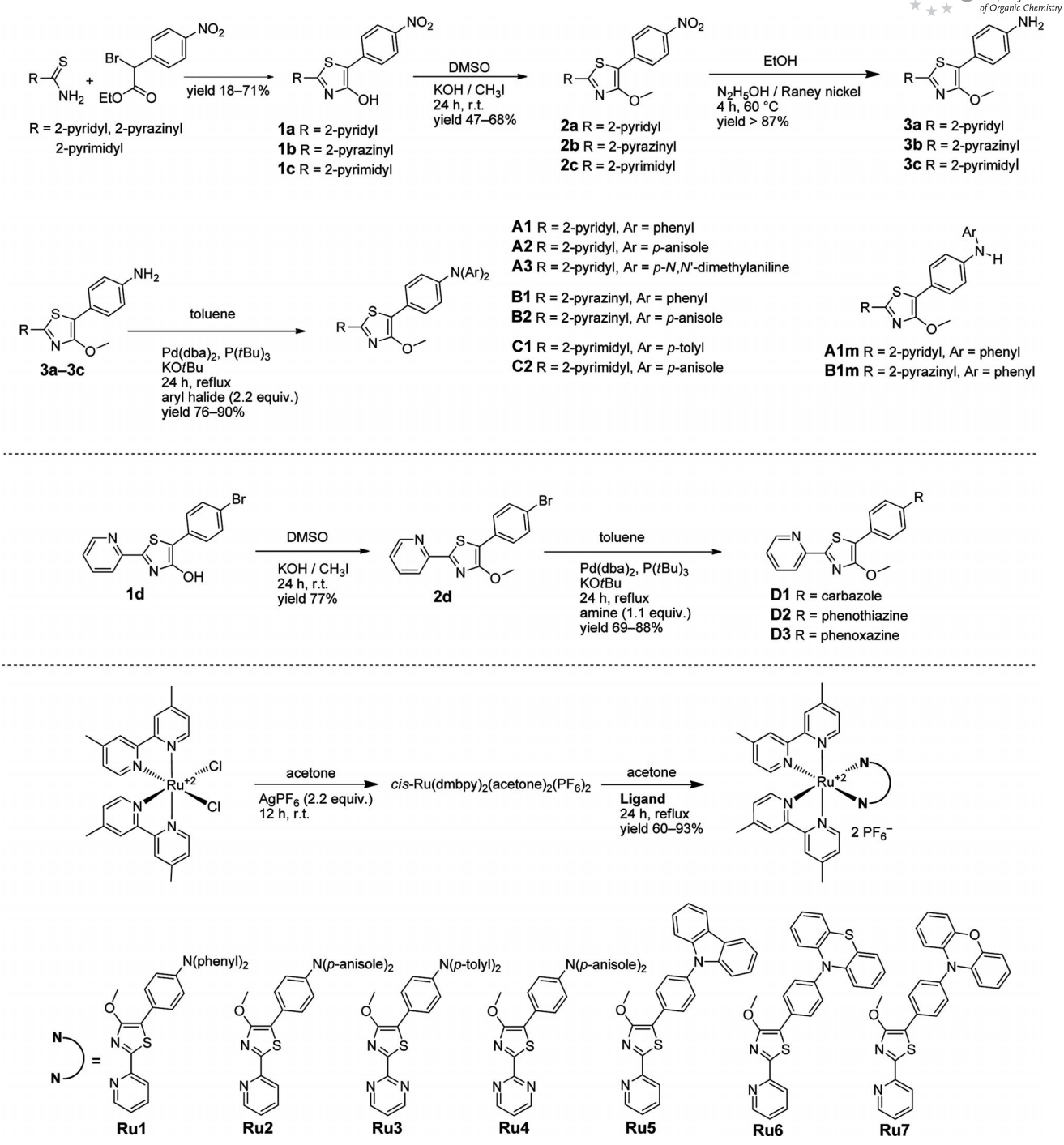

Scheme 1. Synthesis and structure of the ligands and the complexes.

propriate *N*-heterocycle (except for **C1**). The torsion angles are 9.10(7)° for **C1** with the pyrimidine moiety (no hydrogen bond possible) and are decreased to 2.86(6), 7.79(8), and 2.48(9)° for **A1**, **B1**, and **D2**, respectively. Each dye is also twisted to some extent along the 1,3-thiazole-phenyl single bond. Because there is no appreciable steric hindrance it can be assumed that free rotation occurs at room temperature, leading to an unsteady torsion angle in the crystalline state, from almost planar with 9.10(7)° in the case of **C1** to highly twisted with 37.89(10)° in that of **A1**.

The triarylamines display propeller-type geometries of the aromatic rings. They are twisted in a well-known fashion out of the plane into conformations with fewest steric interactions with the adjacent rings, as reported for several arylamines.[25] The nitrogen N3 of the triarylamine in each case adopts an almost planar geometry, in agreement with the sp^2 hybridization and the resulting intramolecular p–π interactions. The interatomic distances and angles both in the arylamine donor and in the 4-methoxy-1,3-thiazole core are all in the expected range.[26] Additionally, the X-ray

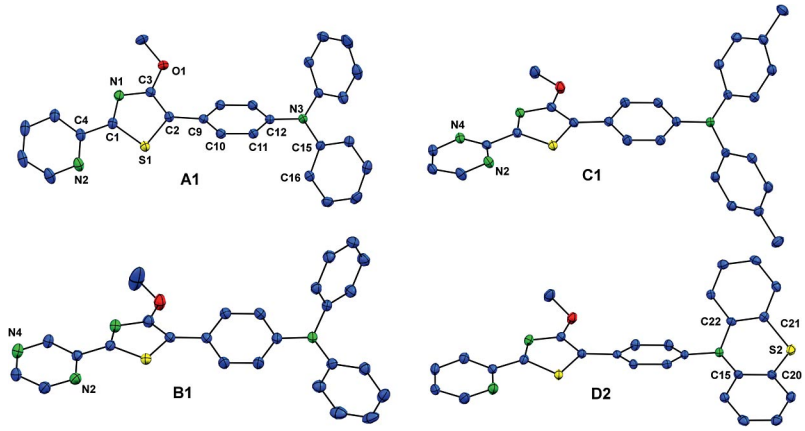

Figure 1. ORTEP plots of the arylamines **A1**, **B1**, **C1**, and **D2**. The numbering of **A1** also applies for the other compounds. Hydrogen atoms are omitted; ellipsoid probability 50%.

Table 1. Selected interatomic distances [Å] and angles [°] in **A1**, **B1**, **C1**, and **D2**.

	A1	B1	C1	D2
Bonds				
N2–C4	1.345(2)	1.342(2)	1.342(2)	1.342(3)
C4–C1	1.467(2)	1.462(2)	1.471(2)	1.463(3)
C1–S1	1.725(1)	1.723(2)	1.725(1)	1.722(2)
S1–C2	1.727(1)	1.733(2)	1.730(1)	1.727(2)
C2–C3	1.376(2)	1.377(2)	1.388(2)	1.383(3)
C3–N1	1.358(2)	1.358(2)	1.359(2)	1.360(3)
C3–O1	1.353(2)	1.355(2)	1.350(2)	1.354(3)
C2–C9	1.467(2)	1.466(2)	1.465(2)	1.468(3)
C12–N3	1.414(2)	1.427(2)	1.417(2)	1.446(3)
Angles				
C1–S1–C2	89.76(6)	89.83(8)	90.17(7)	90.10(10)
S1–C2–C3	107.95(10)	107.70(12)	107.41(10)	107.76(15)
C2–C3–N1	117.56(12)	117.45(15)	117.51(12)	117.40(19)
C3–N1–C1	109.60(11)	109.93(14)	109.89(12)	109.71(18)
N1–C1–S1	115.13(10)	115.08(12)	115.03(10)	115.02(16)
Torsion angles				
N2–C4–C1–S1	2.86(6)	7.79(8)	9.10(7)	2.48(9)
S1–C2–C9–C10	37.89(10)	18.04(12)	1.65(10)	18.47(15)
C11–C12–N3–C15	40.21(11)	62.88(14)	48.35(12)	112.21(18)
C12–N3–C15–C16	34.97(11)	20.10(14)	48.14(12)	6.50(18)

structure of the monosubstituted product **A1m** is given in Scheme S2 in the Supporting Information. It features a geometry very similar to those of the doubly substituted derivatives.

In order to describe the butterfly conformation of the phenothiazine dye **D1**, it is necessary to introduce the folding angle θ and the tilt angle α.

The former refers to the extent of the butterfly conformation, whereas the latter represents the deviation of these planes from coplanarity (α = 0°). For **D1**, θ is 153°, corresponding to α = 27°, which conforms very well with unsubstituted (θ = 159°) or *N*-phenyl-substituted (θ = 155°) phenothiazine.[27] Additionally, the phenothiazine is almost completely twisted out of the plane of the attached phenyl ring [112.21(18)°]. This corroborates the assumption that the annulated arylamines (the same applies for **D1** and **D3**) contribute only marginally to the π-conjugated system, as is also supported by the absorption spectra and quantum chemical calculations.

Electronic Absorption Spectra of the Dyes

The UV/Vis spectra of the ligands are shown in Figure 2 (see also Table 2). Every triarylamine dye shows several high energy transitions below 250 nm where the assignments are tentative (not shown) and two main transitions at 305 and 420 nm. The bands located at 305 nm are due to mixtures of π–π* transitions in the triarylamines. They are not affected either by the donor or by the acceptor. The bands located in the visible part are of charge-transfer (CT) character, as recently shown for similar 4-methoxy-1,3-thiazole dyes.[6] The lowest-energy absorption maxima are influenced both by the donors and by the acceptors. The absorption λ_{max} values are slightly bathochromically shifted by approx. 10 nm for the dyes with the pyrazine instead of the pyridine acceptors. Further shifts of these bands can be observed for the derivatives with more strongly electron-donating arylamines. For **A1**–**A3**, the absorption λ_{max} values are bathochromically shifted from 405 nm for the phenyl- to 417 nm (0.09 eV) for the *p*-anisole-, and further to 433 nm (0.20 eV) for the *p*-*N*,*N*′-dimethylaniline-based triarylamine. This coincides with the behavior of the thiazoles with the pyrazine and pyrimidine acceptor. For compounds **D1**–**D3**, the λ_{max} values of this transition are significantly shifted towards higher energies. This can be explained by the very weak participation of the annulated arylamines in the conjugation pathway, as can be seen from the X-ray structure of **D2**. The extinction coefficients (ε) of the longest-wavelength absorptions are high, varying from 18000 (**D1**) to 30000 $M^{-1}cm^{-1}$ (**B1**). Additionally, the absorption spectra of **D2** and **D3** display a very strong, typical n–π* transition for **D2** (λ = 257 nm, ε = 53000 $M^{-1}cm^{-1}$) and a strong π–π* transition for **D3** (λ = 240, ε = 58000 $M^{-1}cm^{-1}$) for the phenothiazine or phenoxazine moieties, as described for various *N*-aryl-substituted derivatives.[28] The emission spectra of the dyes are depicted in Scheme S3 in the Sup-

porting Information. The emission quantum yields (Φ_F) are also strongly dependent on the arylamine donors. In contrast with the phenyl-based triarylamines, with Φ_F = 40–47%, the *p*-anisole-based triarylamines show Φ_F values below 1%, and consequently no fluorescence was detected for the *p*-*N*,*N*′-dimethylaniline derivative in CH_3CN solution at room temp. The obtained Φ_F values corresponded well with the measured emission lifetimes (τ_F). They were significantly decreased for the compounds with the lower Φ_F values. This prompts the assumption that several radiationless deactivation processes must efficiently depopulate the S_1 state if additional donors (*p*-methoxy **A2**, **B2**, **C2**, *p*-dimethylamino **A3**, or even *p*-methyl **C1**) are present in the triarylamine. More complicated behavior was observed for the derivatives **D1**–**D3**. As a result of the weak overlap of the two chromophores (thiazole and carbazole, phenothiazine, or phenoxazine) the emission spectra are hypsochromically shifted relative to those of the triarylamines **A1**–**A3**. The emission bands for **D2** and **D3** each show several peaks, most likely from transitions into different vibronic states of the electronic ground state. Only one main emission band can be observed for compound **D1** in the polar solvent CH_3CN, with a very high Φ_F of 90%, coincidently with an emission due to the carbazole moiety,[29] whereas for **D2** and **D3** the emissions are very weak.

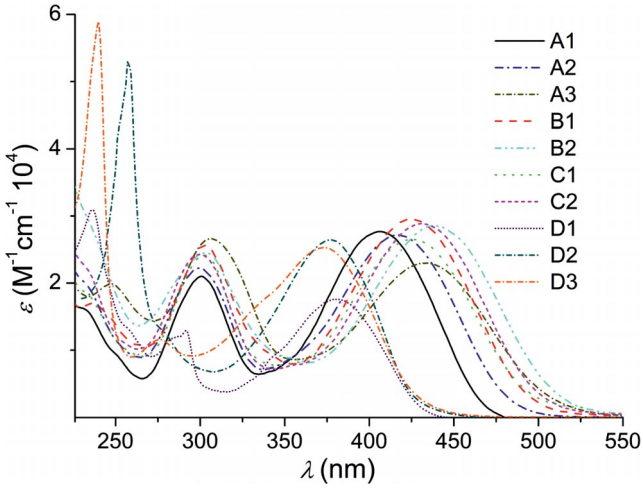

Figure 2. Absorption spectra of the ligands at room temp.

In order to investigate the longest-wavelength absorptions (and emissions) of the dyes in more detail, measurements in different solvents were carried out for compounds **A2** and **D1**. If a simple π–π* transition takes place, both the absorption and the emission maximum should be bathochromically shifted with higher solvent polarities. Surprisingly, it was shown for both compounds (for spectra see Scheme S4 in the Supporting Information) that the absorption λ_{max} values are slightly shifted toward shorter wavelengths with increasing solvent polarity, but the emission maxima are shifted toward longer wavelengths. Consequently, the Stokes shifts increased significantly from 2700 (heptane) to 7400 cm^{-1} (CH_3CN) for **A2** and (less pronounced) from 4300 (heptane) to 5700 cm^{-1} (MeOH) for **D1**. This behavior has been explained in the literature in terms of a conformational transformation from a planar locally excited (LE) state to an intramolecular charge-transfer (ICT) or, consequently, to a twisted intramolecular charge-transfer (TICT) state.[30]

Table 2. Spectroscopic properties of the dyes measured in CH_3CN at room temp.

	λ_{abs} [nm] [log ε]	λ_{em} [nm][a]	Φ_F [%]	τ_F [ns]
A1	301 [4.33], 405 [4.44]	547	47	3.83
A2	299 [4.35], 417 [4.43]	605	<1	0.26
A3	307 [4.43], 433 [4.36]	n.d.	n.d.	n.d.
B1	303 [4.40], 425 [4.47]	593	40	2.99
B2	302 [4.40], 439 [4.46]	611	<1	0.13
C1	302 [4.32], 426 [4.36]	601	8	1.26
C2	301 [4.38], 433 [4.46]	630	<1	< 0.1[c]
D1	292 [4.11], 380 [4.24]	478	90	3.12
D2	257 [4.72], 377 [4.42][b]	484 sh, 507	2	0.11
D3	240 [4.77], 373 [4.40]	455 sh, 470	<1	0.13

[a] λ_{max} of emission after excitation in the maximum of the longest wavelength absorption. [b] Measured in THF. [c] Below demand interval, n.d.: not detected, sh: shoulder.

In our case, the ground-state conformations of the dyes are not planar, as is supported by the X-ray structures. The energies of the S_0 states are basically independent of the solvents used and are only marginally decreased in polar solvents, such as MeOH, leading to small hypsochromic shifts in the absorption spectra for **A2** (Table 3) and **D1** (Table 4). According to the Franck–Condon principle, the geometries of the LE states of S_1 do not change during excitation, leading to very similar energies for these transitions for all solvents. LE states in nonpolar solvents are not stabilized through interactions with solvent molecules, and their conformations are predominately affected by the ground state geometries [sometimes considered partial charge-transfer (PCT) transitions].[12,31] In contrast, the charge-separated ICT states (excitation leads to a formal

Table 3. Spectroscopic behavior of **A2** in different solvents.

Solvent	λ_{abs} [nm] [log ε]	λ_{em} [nm]	Φ_F [%]	Stokes shift [cm^{-1}]	τ_F [ns]
Heptane	427 [4.585]	483, 512	63	3900	2.6
Dioxane	425 [4.441]	530	59	4700	3.8
$CHCl_3$	428 [4.422]	561	40	5500	4.0
THF	425 [4.485]	552	43	5400	3.8
MeOH	421 [4.456]	581	< 1	6500	0.1
CH_3CN	417 [4.434]	603	1	7400	0.1

Table 4. Spectroscopic behavior of **D1** in different solvents.

Solvent	λ_{abs} [nm] [log ε]	λ_{em} [nm] [a]	Φ_F [%]	Stokes shift [cm^{-1}]	τ_F [ns]
Heptane	387 [4.466]	456, 464	97	4300	2.4
Dioxane	385 [4.399]	472	100	4800	2.7
$CHCl_3$	387 [4.235]	475	95	4800	2.9
THF	384 [4.474]	473	100	4900	2.8
CH_3CN	380 [4.244]	475	90	5300	3.1
MeOH	382 [a]	489	81	5700	3.3

[a] Extinction coefficient could not be measured, due to poor solubility.

cation radical at the arylamine and an anion radical at the acceptor) in polar solvents are extraordinarily stabilized by solvent molecules. It is assumed that the ICT transitions are facilitated by planarization along the phenyl-1,3-thiazole bond during the vibrational cooling process (see quantum chemical section). This accounts for the energy gain due to electronic conjugation (mesomeric interactions) and, consequently, the bathochromic shifts of the emission maxima and increased Stokes shifts in solvents with higher polarities. In order to clarify whether a TICT is likely to occur, we used the Lippert–Mataga equation to estimate the change in the dipole moment between S_0 and S_1.[32]

$$\Delta\tilde{\nu} = (\tilde{\nu}_A - \tilde{\nu}_F) = \frac{2}{hc}\left(\frac{\varepsilon - 1}{2\varepsilon + 1} - \frac{n^2 - 1}{2n^2 + 1}\right)\frac{(\Delta\mu)^2}{a^3} + C$$

The Lippert–Mataga plots obtained are shown in Figure 3 and further details are summarized in Scheme S5 in the the Supporting Information. It is known that protic solvents (hydrogen bonding) and 1,4-dioxane do not yield reproducible values,[33] so they were excluded from the analysis. The main uncertainty in this equation is the Onsager cavity radius (a). As described in the pioneering work by Lippert, a was calculated from the major axis of the molecule (simplified as an ellipsoid) and the correction value 0.8 (according to a equal energetic sphere).[34] The lengths of the two molecules can both be derived from the X-ray structures as 17 Å, and the cavity radii are then 13.6 Å. The changes in dipole moment ($\Delta\mu = \mu_E - \mu_G$) were calculated to be 4.6 D for **A2** and 2.8 D for **D1**. This is a strong hint that a planar ICT (PICT) process is taking place rather than a TICT. TICT states usually show significantly higher changes in dipole moments ($\Delta\mu \geq 20$ D) then those observed here.[35]

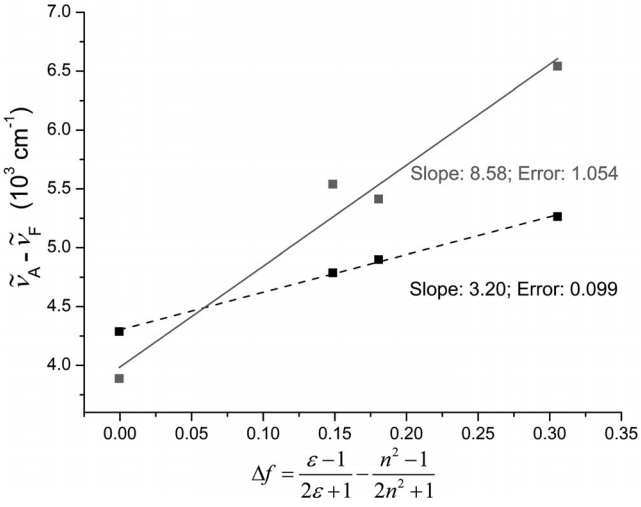

Figure 3. Lippert–Mataga plots for **A1** (solid) and **D2** (dashed). Solvents: heptane, $CHCl_3$, THF, and MeOH, at room temp.

Quantum chemical calculations were carried out in order to evaluate the spatial distributions and energies of the HOMO and LUMO orbitals and whether or not rotations (TICTs) about either the phenyl-1,3-thiazole bonds or the phenyl-amine bonds in the excited states, leading to charge separation, occur. It was found here that the S_1 states are sufficiently stabilized by a polar solvent after planarization along the phenyl-1,3-thiazole bonds, which leads to slightly broadened and red-shifted emission bands, as observed in the UV/Vis measurements. It is noteworthy that no concentration dependencies of either the absorption or the emission spectra were observed, ruling out excimer formation. The bathochromic shifts of the emission are also accompanied by decreased quantum yields and increased emission lifetimes (no clear trend of τ_F was observed for **A1**, unlike for **D2**). Two possible apparently conflictive assumptions can be made to explain this behavior: i) stabilization of the excited state from polar solvent molecules might raise the energy barrier (increased "activation" energy) for the deactivation process (in polar solvents the CT state directly decays radiationlessly to the ground state by the back CT reaction), leading to an increase in τ_F,[31] or ii) various nonradiative quenching processes might be accessible due to additional conformational twists.[30a] The first is consistent with the τ_F measured for **D2**. The second fact was described and discussed in detail by Hu et al. for dyes bearing additional dimethylamino groups on their arylamine donor components (similar to **A3**).[30b] It is assumed that the *p*-dimethylamino (or for **A2** the *p*-methoxy) groups give rise to additional rotatable junctions and radiationless deactivation pathways if the charge-separated states are sufficiently stabilized by polar solvent molecules. The latter explanation would also be consistent with the significantly decreased Φ_F and τ_F values and the lack of emission of the triarylamines in which the donor component is a *p*-dimethylamino, *p*-anisole, or even *p*-tolyl system rather than a phenyl group, as described above. Additionally, it is noteworthy that no wavelength dependency of τ_F was observed in the transient emission spectroscopy for **A2** and **D1** in heptane, ruling out second emissive states (dual fluorescence).

Electronic Absorption Spectra of the Ru^{II} Complexes

The studied complexes each show several intense absorption bands due to the different possible electronic transitions of Ru^{II} polypyridyl complexes. The spectra are shown in Figure 4 and the data are summarized in Table 5. The high-energy bands at 258 nm can be assigned to spin-allowed metal-to-ligand charge-transfer (MLCT) transitions. The intense ligand-centered (LC) π–π* transitions ($\varepsilon >$ 65000 $M^{-1}cm^{-1}$) of the two dmbpy ligands are located at 285 nm. The high-energy LC transitions of the triarylamines **A1**–**C2** can be observed at approximately 325 nm, and they are presumably superimposed with weak metal-centered (MC) transitions.[9a]

The broad absorption bands of the complexes in the visible region at 400–600 nm are due to MLCT transitions and LC transitions of the thiazole-based ligands. It is not possible to assign any distinct transition to these broad featureless bands ($\varepsilon >$ 28000 $M^{-1}cm^{-1}$) for the complexes **Ru1**–**Ru4**. For **Ru5**–**Ru7** the different transitions are better resolved. The bands of the LC transitions for **Ru5**, **Ru6**, and **Ru7** are

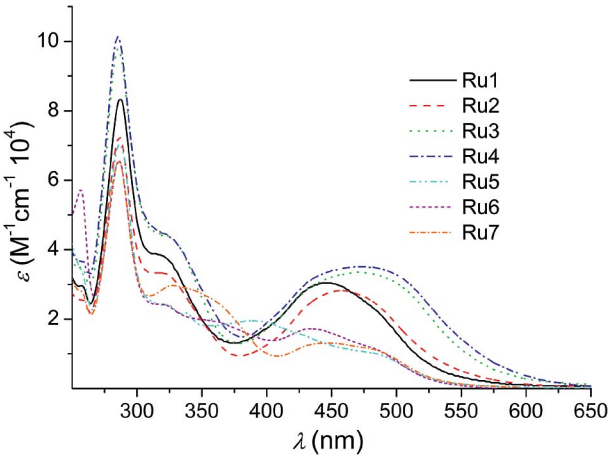

Figure 4. Absorption spectra of the complexes measured in CH_3CN at room temp.

Table 5. Spectroscopic properties of the complexes measured in CH_3CN at room temp.

	λ_{abs} [nm] [log ε]	λ_{em} [nm][a]
Ru1	258 [4.47], 287 [4.92], 319 [4.59], 447 [4.48]	606, 689
Ru2	258 [4.41], 286 [4.86], 324 [4.52], 457 [4.45]	619, 710
Ru3	258 [4.54], 285 [4.99], 326 [4.64], 471 [4.53]	629, 727
Ru4	258 [4.57], 285 [5.00], 328 [4.63], 473 [4.55]	627, 736
Ru5	258 [4.52], 286 [4.85], 389 [4.29], 486 [4.00]	676
Ru6	286 [4.82], 362 [4.29], 434 [4.24], 485 [4.05]	679
Ru7	286 [4.82], 327 [4.47], 446 [4.12], 483 [4.05]	667

[a] Measured in ethanol/methanol (4:1, v/v) glass at 77 K after excitation at 450 nm.

located at 390, 370, and 360 nm (broad), respectively. This is in accordance with the absorption maxima of the free ligands and leads to the conclusion that the longest-wavelength ligand-based CT transitions are marginally affected by complexation. The bands of the MLCT transitions to the dmbpy ligand are located at approx. 435 nm. Unlike those for **Ru1**–**Ru4**, the MLCT bands for the three complexes **Ru5**–**Ru7** are acceptably resolved and each display an additional shoulder located at 490 nm. This can be explained by absorption into two different ^{1}MLCT states caused by the presence of two different ligands (the thiazole-based and the dmbpy ligands).[36]

In conclusion, as a result of the complexation of the additional light-absorbing ligands, leading to several intense bands in the absorption spectra of the complexes superimposed with the "classic" transitions, the complexes show enhanced light-harvesting efficiencies in the UV/Vis and visible regions of the solar spectrum.

Unlike the very similar thiazole-based complexes described in the literature,[8] the compounds do not show any room temperature emission, so emission spectroscopy was carried out in EtOH/MeOH (4:1, v/v) glass at 77 K. The measured complexes each exhibit emission between 606 and 736 nm. For complexes **Ru1**–**Ru4**, with the triarylamine-based ligands, two different main emission bands can be observed in each case, whereas for **Ru5**–**Ru7** only one main emission band is present. The emission spectra of **Ru1**, **Ru2**, **Ru5**, and **Ru6** are shown as representative examples in Figure 5. The unexpected behavior of **Ru1**–**Ru4**, although it violates Kasha's rule, is not new (especially at a temperature of 77 K) and has been described in the literature. Two possible mechanisms have been discussed as an explanation. Firstly, two emitting ^{3}MLCT states might be present, as documented for, for example, heteroleptic Ru^{II} complexes containing two bpy and one 2,3-bis(2-pyridyl)pyrazine ligand[37] or two bpy and different phenanthroline-based ligands[38] or for acetylene-linked dinuclear Ru^{II} complexes.[39] This behavior can usually be assigned only by time-resolved emission dynamics measurements, due to the superimposition of the two emission bands. Secondly, one emitting ^{3}MLCT and one emitting ligand localized triplet excited state (^{3}IL) might be present, as extensively discussed in a review by Wang et al.[40]

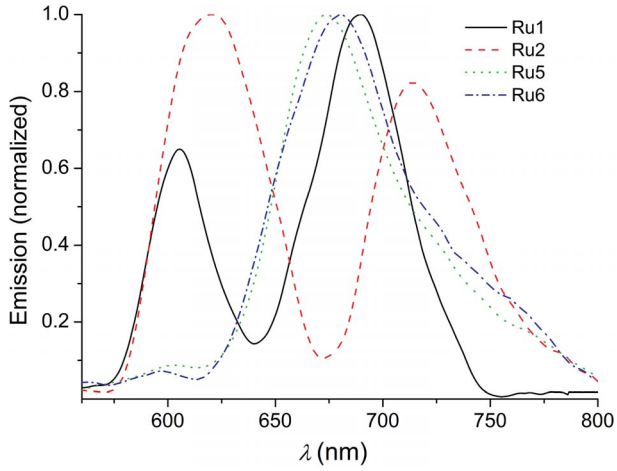

Figure 5. Emission spectra of the heteroleptic Ru^{II} complexes **Ru1**, **Ru2**, **Ru5**, and **Ru6** in ethanol/methanol (4:1, v/v) glass at 77 K.

In the cases of the complexes **Ru1**–**Ru4** the two bands are well resolved. Excitation at 400 nm leads in each case to an increase in the intensity of the higher-energy emission at approx. 620 nm whereas excitation at the longest-wavelength absorption >500 nm leads to an increase in the lower-energy emission band at approx. 710 nm. Two different emitting states separated by a distinct energy barrier are populated in a manner dependent on the excitation wavelength, as was also supported by measurement of excitation spectra. We assume that one of these emissive states is of ^{3}MLCT character and is localized on a dmbpy–Ru pair and that the other is the lower-energy ^{3}MLCT state localized on the thiazole–Ru pair and not a ^{3}IL state. The latter assumption is also supported by measurement of the emission spectra of the ligands. The locations and differences of the maxima of/and between the ligands do not fit with either the short- or the long-wave emissions of the complexes. Nonetheless, unambiguous assignment will be the subject of further time-dependent measurements carried out at 77 K. For the complexes **Ru5**–**Ru7** only one broad emission band is apparent in each case. Presumably the energies of the two possible ^{3}MLCT states are too close, which

would lead to superimposed emission bands, in contrast with the absorption spectra, in which the two different ^{1}MLCT transitions are well resolved.

Quantum Chemical Calculations on A1 and D1

In order to gain more detailed insight into the structural and the spectroscopic properties of **D1** and **A2**, density functional theory (DFT) and its time-dependent variant (TDDFT)[41] were applied. The influence of solvation was studied for an apolar (heptane, ε = 1.9113, n = 1.3878) and a polar (MeOH, ε = 32.613, n = 1.3288) solvent with use of a polarized continuum model.[42] All calculations were performed with the GAUSSIAN 09 program.[43] The ground-state equilibrium structures of **A2** and **D1** were optimized with a functional based on B3LYP[44] and denoted as B3LYP(35),[45] combining 35% of exact exchange, 58.5% of non-local B88[46] exchange, and the LYP correlation along with the 6–31G(d,p) double-ξ basis set.[47] Harmonic vibrational frequencies at the same level of theory confirmed that the obtained stationary points corresponded to the minima of the potential energy surfaces (PESs). Excited state properties, such as excitation energies, oscillator strengths, and excited states geometries, were computed by use of TDDFT and the same exchange-correlation functional and basis set as for the ground states. The absorption spectra in the Franck–Condon (FC) region were simulated from the first ten singlet excited states. The S_1 states were optimized to obtain the emission energies. Furthermore, PESs of the S_0 and the S_1 states of **A2** were generated along the dihedral angle δ_4 (starting from the optimized S_1 geometries for heptane and MeOH), describing the internal torsion of the donor group (for a graphic representation of the angles see Scheme S6 in the Supporting Information) in order to study the presence of a TICT state in the S_1 state. The PESs were calculated with rotation of the phenyl group with respect to the bis(4-methoxyphenyl)-*N*-phenylaniline moiety with a step size of 2° and at the same level of theory as the previous calculations.

The ground-state equilibrium geometries of both molecules exhibit similar structural features, as shown in Table 6 and Figure 6. The *trans* isomer of the thiazole-pyridine moiety is in each case energetically favored over the *cis* isomer by approximately 0.3 eV in heptane and by 0.2 eV in MeOH. As can be seen from the dihedral angles, the 4-methoxy-1,3-thiazole fragment adopts a configuration almost planar to the pyridine. The angle δ_2 describes the torsion around the C–C bond between the thiazole fragment and the donor moiety. It was found that δ_2 is almost independent both of the donor group [carbazole and bis(4-methoxyphenyl)-*N*-phenylaniline] and of the solvent (for **A2** δ_2 = 18° in heptane and 19° in MeOH, whereas for **D1** δ_2 = 17° in both solvents). The phenyl groups of the donor in both dyes are twisted out of planarity due to steric hindrance. This twisting is in the range of ca. 30°, as illustrated by the angles δ_3 and δ_4 in **A2**. The torsion of the carbazole in the case of **D1** is significantly more pronounced (δ_3 = 56°), whereas the carbazole is completely planar. In general, and consistently with the results of the solvent-dependent UV/Vis measurements, the ground-state structures of **A2** and **D1** are basically invariant to solvation. The optimized geometries of the S_1 states show similarities to the ground-state equilibrium structures. The reason is the π–π* nature of the S_1 states and the partial occupation of the LUMOs; the excited-state structures therefore show only minor shifts in bond lengths and angles. The thiazole-phenyl fragments, however, are planarized ($\delta_2 \approx -1°$ for **A2** and 2° for **D1**) as

Table 6. Calculated torsion angles and dipole moments of the ground (S_0) and first excited (S_1) states of **A2** and $\mathbf{D_1}$.

Geom.	Solvent	δ_1 [°]	δ_2 [°]	δ_3 [°]	δ_4 [°]	μ [D]
A2						
S_0	heptane	0.32	–17.99	30.61	31.56	1.37
	MeOH	0.34	–19.01	28.09	29.67	1.55
S_1	heptane	–0.43	–1.19	39.11	38.30	1.58
	MeOH	–0.32	–1.58	32.68	32.10	2.62
D1						
S_0	heptane	0.03	–16.65	56.42	–0.09	5.38
	MeOH	0.00	–17.32	56.54	–0.12	6.12
S_1	heptane	–0.22	–2.22	44.39	–0.09	4.64
	MeOH	–0.27	–2.02	45.46	0.00	5.22

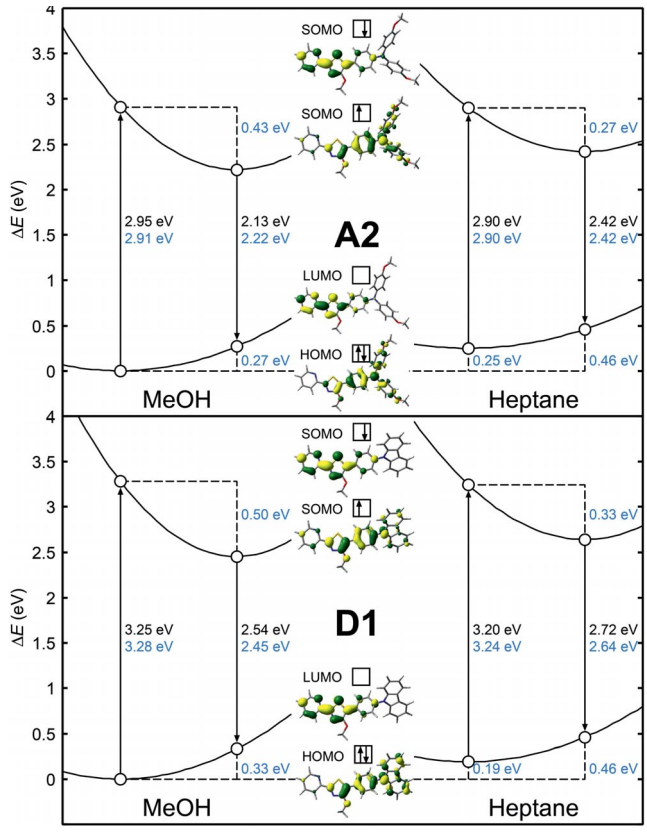

Figure 6. Potential curves, representations of the HOMO, LUMO, and SOMO orbitals, and energies of the S_0 and S_1 states before and after stabilization through either heptane or MeOH solvent molecules and experimentally determined (upper values of the absorption and emission energies) and calculated energies.

a result of the bonding characters of the LUMOs in these positions. Additionally, the torsions in the donor groups are slightly changed. In the case of **D1**, the angle δ_3 decreases by approximately 12 to 44° in heptane and to 45° in MeOH. This supports the assumption that excitation leads to a PICT and not a TICT state.

The absorption spectra of the two dyes were calculated by using FC geometries and the first ten singlet excited states. Table 7 lists the vertical and adiabatic S_1 excitations for the compounds in both solvents. A summary of the photophysical properties and a representation of the orbitals of the higher excited singlet states are given in Schemes S7–S10 in the Supporting Information. The S_1 state of **D1** is mainly characterized by a π–π* excitation with significant CT participation predominantly from the carbazole donor (HOMO) to the thiazole/pyridine acceptor (LUMO). The ratio of this transition in heptane is 87% and it is slightly enhanced to 89% in MeOH. An additional π–π* transition of **D1** from the HOMO–1 to the LUMO shows a significant weight of 11% (heptane) and 9% (MeOH).

Table 7. Calculated absorption/emission properties to/from the first singlet excited states S_1. Main contributions to the wave function (weight), vertical (absorption) or adiabatic (emission) excitation energies (ΔE^e in eV and nm), oscillator strengths (f), and deviations from experimental results ($\Delta\Delta E_{Exp}$). H: HOMO, L: LUMO.

	Solvent	Transition	Weight [%]	ΔE^e [eV]	[nm]	f	$\Delta\Delta E_{exp}$ [eV]
A2							
Abs.	heptane	H→L	94	2.90	428	1.021	0.00
		H–1→L	4				
	MeOH	H→L	94	2.91	426	1.006	–0.04
		H–1→L	4				
Em.	heptane	H←L	96	2.42	512	1.088	0.00
	MeOH	H←L	96	2.22	559	1.341	0.09
D1							
Abs.	heptane	H→L	87	3.24	382	0.986	0.04
		H–1→L	11				
	MeOH	H→L	89	3.28	378	0.995	0.03
		H–1→L	9				
Em.	heptane	H←L	97	2.64	469	1.137	–0.08
	MeOH	H←L	97	2.45	506	1.306	–0.09

The HOMO–1/LUMO transition has a less pronounced CT character than the HOMO/LUMO transition, because the HOMO–1 is delocalized over the entire molecule. On the other hand, the S_1 state of **A2** has a weighting of 94% in favor of the HOMO/LUMO transition (heptane and MeOH), whereas the HOMO–1/LUMO transition only has a weighting of 4%.

In conclusion, the S_1 state of **A2** has a more pronounced CT character than that of **D1**. The wavelength dependency of the first absorption band on solvent polarities is in very good agreement with the experimental findings (Table 7, Figure 6). The excitation energies of the S_1 states are marginally overestimated by 0.04 eV or underestimated by –0.04 eV, respectively, showing that the B3LYP(35) functional is very well suited to describe the CT in these dyes in both polar and apolar solvents. Comparison of the oscillator strengths (f) with the experimentally observed ε values shows that they are constant for **A2** and **D1** in both solvents. The trend of decreasing ε values with increasing solvent polarity was also reproduced in the electronic structure calculations.

The adiabatic emission spectra were obtained by use of the optimized geometries of the first excited singlet states. The vertical emissions to the S_0 were calculated by use of these structures. The fluorescence energies, measured and simulated, are listed in Table 7. The energies obtained are in excellent agreement with the experimental findings. In the case of **A2**, the divergences from the simulations to the experimentally determined values are 0.00 (heptane) and 0.09 eV (MeOH), whereas for **D1** they are –0.09 (MeOH) and –0.08 eV (heptane). Relaxation in the S_1 state leads to a wave function with a significantly increased weight of the HOMO/LUMO transition. A similar trend was observed for the two chromophores. In the case of **A2**, the weight, the CT nature of the S_1 state, of the HOMO/LUMO transition increases from 94 to 96%, whereas for **D1** it rises from 87 (heptane) and 89% (MeOH) to 97% in both solvents. This can be explained in terms of the planarization in the dihedral angle δ_2, which leads to a greater amount of CT character for this transition. The energy of the S_1 state is substantially dependent on the solvent; the polar solvent stabilizes the excited state considerably, by 0.43 and 0.50 eV for **A2** and **D1**, respectively, whereas the apolar solvent stabilizes the S_1 by only 0.27 and 0.33 eV, respectively. The significant difference in the emission energies in heptane and in MeOH can be explained in terms of the enhanced weight of the HOMO/LUMO transition in the S_1 wave function of the planarized geometry.

Further investigations were carried out in order to study the likelihood of PICT or TICT states. The optimization in the S_1 states did not affect the arrangements of the donor groups drastically (see δ_3 and δ_4), leading to the conclusion that no TICT state is observed in these dyes. However, the TICT is not connected to a barrier-free evolution in the excited state PES, as described in the literature, so a scan of the S_0 and the S_1 states around the dihedral angle δ_4 was performed for the chromophore **A2**. The PESs obtained for both solvents are depicted in Figure 7. The minima of the ground states in both solvents are found at approx. 30 and 210°. These minima are separated by barriers of 1.87 (MeOH) and even 2.55 eV (heptane). The excited state PESs show similar behavior: the minima here are located at ca. 34 (MeOH) and 38° (heptane), values consistent with the angles in the optimized S_1 geometries of **A2**. The PESs of the S_1 state are almost parallel to those of the electronic ground state and no evidence for a minimum at 90° was found. In order to support this statement an additional optimization procedure was performed with a starting torsion of δ_4 of 90°. However, the obtained structure evolved to that of the optimized geometry at the FC region. In summary, the appearance of a TICT state in this chromophore can be excluded from the quantum chemical calculations.

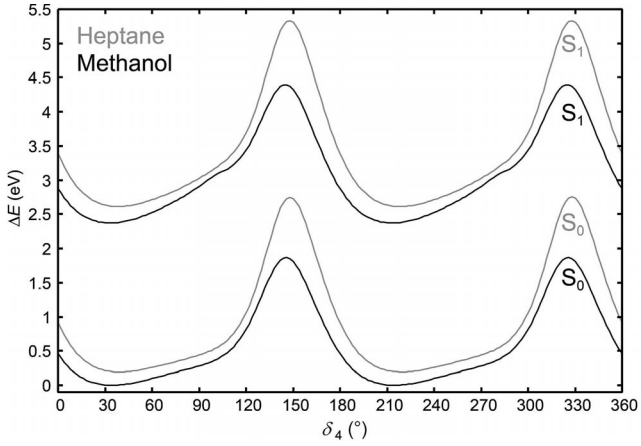

Figure 7. Scan around the dihedral angle δ_4 for **A2**.

Electrochemical Properties of the Dyes

Electrochemical measurements were carried out with CH_3CN as solvent, with platinum as counter, Ag/AgCl as reference, and carbon as working electrodes, and with tetrabutylammonium hexafluorophosphate ($TBAPF_6$) as the conducting salt (scan rate 0.2 $V s^{-1}$). Ferrocene was added as the internal standard after every measurement. All values discussed here are relative to the Fc/Fc^+ redox couple and the data are listed in Table 8. The cyclic voltammetry (CV) spectra of **A1**–**A3** are depicted as representative examples in Figure 8 (spectra of the other compounds can be found in Scheme S11 in the Supporting Information). For these types of compounds it is known that the first oxidations occur at the triarylamine components, leading to the formation of positively charged cation species.[48] Each dye therefore shows a first reversible oxidation wave that is strongly influenced by the electronic properties of the arylamine. No reactions of the radical cations or dications of the triarylamines to form σ-dimers with additional discharging waves at more negative potentials (at ca. –1.0 V) or carbazole derivatives with additional discharging waves at 0.7 V were detected under the conditions used.[49] The half-wave potentials ($E_{1/2}$) of the first oxidation are 0.23–0.26 V for the arylamines **A2**, **B2**, and **C2**, with the strongly electron-donating 4-methoxyphenyl groups, 0.36 V for arylamine **C1**, with the 4-tolyl substituents, and 0.41 and 0.43 V for the triphenylamines **A1** and **B1**, respectively. For **A3**, with the very strongly electron-donating dimethylamine groups on the arylamine, the oxidation potential is significantly lowered to –0.17 V. This is consistent with the observation that this compound is already oxidized by atmospheric O_2 in solution ($CDCl_3$, reduction of the cation radical with Zn in an NMR tube; see Scheme S12 in the Supporting Information). Additionally, **A3** shows a reversible second oxidation wave due to the formation of a doubly-charged quinoid bication at 0.13 V,[50] whereas all other triarylamines exhibit second irreversible oxidation waves. The $E_{1/2}$ values for these second oxidations are located in a very small range of 0.66–0.77 V and are independent of the triarylamine components. The oxidation wave for the carbazole-derived dye **D1** is completely irreversible, due to the coupling of the cation radical in *para*-position.[51] The half-wave potential ($E_{1/2}$) is 0.84 V, which is in accordance with examples in the literature.[52] For the phenothiazine-based dye **D2** the oxidation wave is reversible. The $E_{1/2}$ is 0.31 V vs. Fc/Fc^+ or 0.68 V vs. the reference electrode used (Ag/AgCl, KCl, 0.1 M). This is consistent with the electronically similar arylamine 10-phenylphenothiazine (0.88 V vs. Ag/AgCl, sat. KCl) and with other phenothiazines reported in the literature.[53]

Table 8. Electrochemical data for the donor–acceptor dyes and the Ru^{II} complexes.

Dye	$E_{1/2,ox}$ [V][a]	$E_{1/2,red}$ [V][a]	E^{HOMO} [eV][b]	E^{LUMO} [eV][b]	ΔE^{cv} [eV][b]	E_g^{opt} [eV][c]
A1	0.41, 0.73[d]	–2.19	–5.19	–2.74	2.45	2.67
A2	0.23, 0.66[d]	–2.23	–5.02	–2.74	2.28	2.57
A3	–0.17, 0.13	–2.25	–4.56	–2.62	1.94	2.42
B1	0.43, 0.77[d]	–1.97	–5.22	–2.96	2.26	2.54
B2	0.26, 0.77[d]	–1.98	–5.06	–2.95	2.11	2.44
C1	0.36, 0.76[d]	–2.03	–5.16	–2.90	2.26	2.51
C2	0.25, 0.77[d]	–2.05	–5.05	–2.88	2.17	2.49
D1	0.84 [d]	–2.15	–5.65	–2.78	2.87	2.85
D2	0.31, 1.05[d]	–2.11	–5.09	–2.87	2.22	2.93
D3	0.34, 1.00[d]	–2,14	–5.07	–2.74	2.33	2.92
Complex						
Ru1	0.61, 0.83	–1.58, –1.98, –2.21	–5.37	–3.34	2.03	2.32
Ru2	0.36, 0.83	–1.61, –1.97, –2.20	–5.16	–3.32	1.84	2.25
Ru3	0.52, 0.90	–1.42, –1.95, –2.14	–5.33	–3.52	1.81	2.13
Ru4	0.37, 0.89	–1.44, –1.96, –2.16	–5.14	–3.51	1.63	2.09
Ru5	0.80[d], 0.85	–1.53, –1.94, –2.18	–5.61	–3.41	2.20	2.39
Ru6	0.33, 0.81	–1.53, –1.97, –2.19	–5.13	–3.41	1.77	2.32
Ru7	0.34, 0.82	–1.52, –1.98, –2.19	–5.07	–3.35	1.72	2.26

[a] Measurements were performed in CH_3CN containing $TBAPF_6$ (0.1 M). The potentials are given vs. ferrocene/ferrocenium (Fc/Fc^+). [b] Determined by use of $E^{HOMO} = -[(E_{onset,\,ox} - E_{onset,\,Fc/Fc+}) - 4.8]$ eV and $E^{LUMO} = -[(E_{onset,\,red} - E_{onset,\,Fc/Fc+}) - 4.8]$ eV.[59] [c] Estimated from the UV/Vis spectra at 10% of the maximum of the longest-wavelength absorption band on the low-energy side. [d] Derived from differential pulse polarographic measurements; peaks are irreversible.

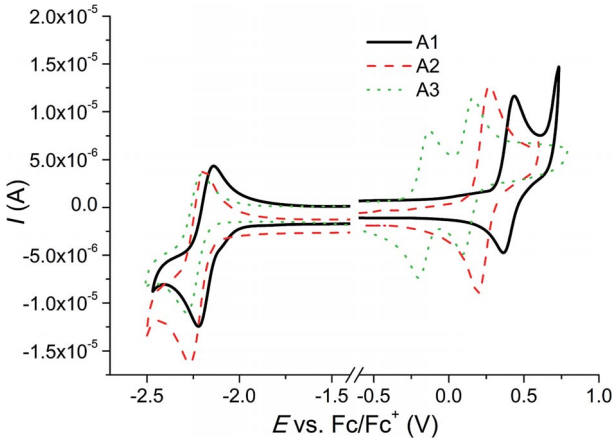

Figure 8. Cyclic voltammetry of dyes **A1**–**A3**. Experimental conditions: 0.1 M $TBAPF_6/CH_3CN$ solution, $c \approx 1 \times 10^{-4}$ M, room temp., scan rate 0.2 $V s^{-1}$. RE: Ag/AgCl. WE: carbon. AE: platinum.

The first oxidation wave for **D3** is also reversible and is located at 0.34 V, consistently with an oxidation of the phenoxazine.[54] The similar $E_{1/2}$ values for **D2** and **D3** are in accordance with the very similar electronic behavior of phenothiazine and phenoxazine.[55] Additionally, **D2** and **D3** each show a second irreversible oxidation wave located at approx. 1.0 V.

All dyes show reversible first reductions. The $E_{1/2}$ values of the first reduction are slightly dependent on the acceptors and not on the arylamines. The redox potentials vary from –2.19 to –2.25 V for the dyes with the pyridine acceptor (**A1**–**A3**). They are shifted to more positive potentials (the reduction is facilitated) when the electron deficiency of the acceptor is increased. The reductions occur at ca. –1.97 V for the dyes **B1** and **B2** and at –2.03 and –2.05 V for **C1** and **C2**, respectively. It can therefore be assumed that the reductions each take place at the acceptor, leading to a negatively charged azabenzene, as described in the literature.[56] Irreversible reduction due to proton abstraction of the radical anion from residual water, to form a free radical that would be immediately reduced at the potential of its formation,[57] was not observed (the measurements were carried out under water-free conditions).

Electrochemical Properties of the Ru^{II} Complexes

The complexes **Ru1**–**Ru7** were characterized by CV under the same conditions as discussed above. The electrochemical results are presented in Table 8 and the spectra of **Ru1**, **Ru2**, **Ru5**, and **Ru6** are given as representative examples in Figure 9 (spectra of the other compounds can be found in Scheme S13 in the Supporting Information). They each show two reversible oxidation waves (except **Ru5**) and three reversible reduction waves. The former can be attributed to oxidation of the arylamines and of the Ru^{II} ruthenium center to Ru^{III}.[58] The oxidations of the arylamines of the coordinated ligands are marginally shifted towards higher potentials relative to the free dyes, confirming the assumption that the corresponding ligand-centered π-orbitals are lowered in energy after complexation. The Ru^{II}/Ru^{III} oxidations are shifted slightly towards higher potentials for the thiazoles with pyrimidine rather than pyridine acceptor moieties, due to the more strongly electron-accepting properties of the pyrimidine, lowering the energies of the t_{2g} orbitals. The three reversible reduction waves are well resolved in each case and are located at approx. –1.42 to –1.61, –2.0, and –2.2 V. No clear trend is obvious, and assignment to reduction of the ligand-located antibonding π*-orbitals of either a thiazole or dmbpy ligand would be tentative. Additionally, behavior similar to that of **A3** was found for the complex **Ru4**. The signals of the arylamine protons are extremely broadened in the ^1H NMR spectra due to partial formation of the radical cation in aerated CD_3CN solution (see Scheme S14 in the Supporting Information). The signals became well resolved after the addition of Zn and reduction of the cation radical.

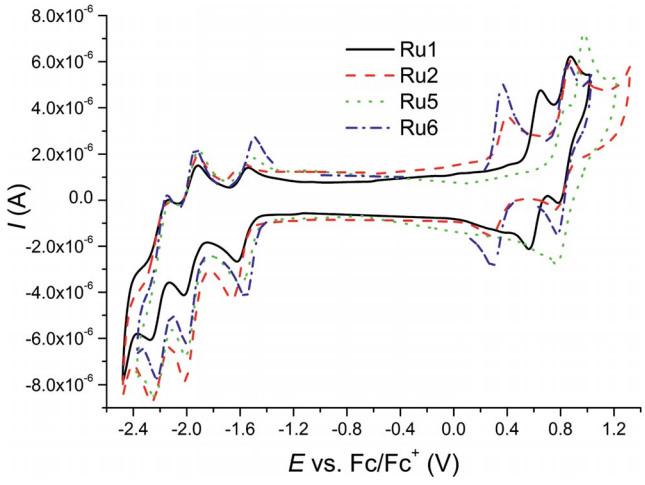

Figure 9. Cyclic voltammetry of **Ru1**, **Ru2**, **Ru5**, and **Ru6**. Experimental conditions: 0.1 M $TBAPF_6/CH_3CN$ solution, $c \approx 5 \times 10^{-5}$ M, room temp., scan rate 0.2 $V s^{-1}$. RE: Ag/AgCl. WE: carbon. AE: platinum.

Conclusions

A series of donor–acceptor dyes featuring different arylamines moieties as electron donating units have been successfully prepared by a Buchwald–Hartwig cross-coupling approach. Different azaheterocycles were employed as acceptor moieties. The spectroscopic and electrochemical properties, as well as the HOMO/LUMO gaps, of these dipolar compounds are significantly affected by the different donors used. The natures of the intramolecular charge-transfer states were identified as PICT processes for one of the triarylamine-based (**A2**) and one of the tricyclic arylamine dyes (**D1**) with the aid of spectroscopic methods and quantum chemical calculations. Furthermore, the absorption and emission spectra and energies of the transitions, oscillator strengths, and weights were calculated for the optimized ground- and excited-state structures of these two dyes. The synthesis and characterization of the corresponding Ru^{II} polypyridyl complexes of seven of the dyes/ligands

are reported. Each complex shows an enhanced absorption in the visible part of the UV/Vis spectrum, due to additional LC and MLCT transitions originating from 4-methoxy-1,3-thiazole ligands. All compounds were unambiguously identified by NMR spectroscopy, elemental analysis, mass spectrometry, and MALDI-TOF measurements. Further research into the presented dyes will focus on the synthesis of the analogous Ru(dcbpy)(**L**)$(SCN)_2$ (dcbpy = 2,2′-bipyridine-4,4′-dicarboxylic acid) for DSSC applications. The dyes will also be tested with regard to their two-photon excitation behavior, which could open doorways to several new applications such as two-photon excitation microscopy. First tests established this ability for a dye with a methoxy donor group similar to **A1**.

Experimental Section

Ethyl 2-bromo-2-(4-nitrophenyl)acetate and 5-(4-bromophenyl)-2-(pyridin-2-yl)thiazol-4-ol (**1d**) were synthesized by literature procedures.[18–19] Pyridine-2-carbothioamide, pyrazine-2-carbothioamide, and pyrimidine-2-carbothioamide are commercially available or can be prepared from the corresponding nitriles and H_2S. $Pd(dba)_2$ and $P(tBu)_3$ (1 M solution in toluene) were purchased from Sigma–Aldrich. $Ru(dmbpy)_2Cl_2$ was prepared with use of microwave irradiation by a literature procedure and was readily purified by column chromatography (Al_2O_3 activity 10, CH_2Cl_2 to CH_2Cl_2/MeOH 50:1 as eluent).[60] All other chemicals used were reagent grade and purchased from Sigma–Aldrich or Acros. Solvents were purified by standard procedures. Solvents for UV/Vis, emission spectroscopy, and CV were of analytical grade and bought from Sigma–Aldrich. ^1H and ^{13}C NMR and the corresponding correlation spectra were recorded with Bruker AC-250 (250 MHz) and AC-400 (400 MHz) spectrometers. Chemical shifts (δ) are given relative to solvents. UV/Vis data for the compounds were collected with a Lambda 19 instrument from Perkin–Elmer and emission spectra were measured with a Jasco FP 6500 instrument. Quantum yields were determined relative to fluorescein (NaOH, 0.1N, Φ_F = 0.82) with refractive indices n(NaOH) = 1.334 and $n(CH_3CN)$ = 1.344.[35d] Elemental analysis was carried out with a Leco CHNS-932 instrument. Mass spectra were measured either with a Finnigan MAT SSQ 710 (EI) or a MAZ 95 XL (FAB) system. MALDI-TOF MS was performed with a Bruker Ultraflex TOF/TOF mass spectrometer fitted with a 337 nm nitrogen laser operated in the reflectron mode with an acceleration voltage of 25 kV. Dithranol was used as matrix. Electrochemical measurements were performed with a Metrohm Autolab PGSTAT30 potentiostat with a standard three-electrode configuration. The experiments were carried out in degassed solvents containing Bu_4NPF_6 salt (0.1 M). At the end of each measurement ferrocene (Fc/Fc^+) was added as an internal standard. TLC materials were from Merck (Polygram SIL G/UV254, aluminum oxide 60 F254). The material for column chromatography was also obtained from Merck (silica gel 60).

Structure Determinations: The intensity data for the compounds were collected with a Nonius KappaCCD diffractometer and use of graphite-monochromated Mo-K_α radiation. Data were corrected for Lorentz and polarization effects but not for absorption effects.[61] The structures were solved by direct methods (SHELXS)[62] and refined by full-matrix, least-squares techniques against F_o^2 (SHELXL-97).[62] The hydrogen atoms of **B1** (without the methyl group hydrogen atoms at C4), **C1**, and **D2** and the amine hydrogen atom at N3 of **A1m** were located by difference Fourier synthesis and refined isotropically. The hydrogen atoms of **A1** and **A1m** were included at calculated positions with fixed thermal parameters. All non-hydrogen atoms were refined anisotropically.[62] Crystallographic data and structure solution and refinement details are summarized in Table 1. XP (SIEMENS Analytical X-ray Instruments, Inc.) was used for structure representations. CCDC-876513 (for **A1**), -879865 (for **A1m**), -876514 (for **B1**), -876515 (for **C1**), and -876516 (for **D2**) contain the supplementary crystallographic data for this paper. These data can be obtained free of charge from The Cambridge Crystallographic Data Centre via www.ccdc.cam.ac.uk/data_request/cif.

5-(4-Nitrophenyl)-2-(pyridin-2-yl)thiazol-4-ol (1a): A suspension of pyridine-2-carbothioamide (1.00 g, 7.24 mmol), ethyl 2-bromo-2-(4-nitrophenyl)acetate (2.50 g, 8.68 mmol, 1.2 equiv.), and pyridine (8.58 g, 10.8 mmol, 2 equiv.) in toluene (100 mL) was stirred under reflux for six hours and a yellow fluffy precipitate was produced. After the system had cooled to room temperature, the precipitate was filtered off, washed with EtOH and Et_2O, and dried in vacuo; yield 3.05 g (10.2 mmol, 71%). ^1H NMR (400 MHz, [D$_6$]DMSO): δ = 12.44 (s, 1 H), 8.65 (d, J = 4.4 Hz, 1 H), 8.24 (d, J = 8.9 Hz, 2 H), 8.07–7.94 (m, 4 H), 7.52 (t, J = 5.5 Hz, 1 H) ppm. ^{13}C NMR (100 MHz, [D$_6$]DMSO): 164.0, 161.6, 150.4, 150.0, 145.0, 139.5, 138.4, 126.7, 126.0, 124.7, 119.3, 108.8 ppm. UV/Vis (DMSO): λ_{max} [log(ε/M^{-1} cm^{-1})] = 414 [4.40], 609 [3.64] nm. MS (EI): m/z (%) = 299 (100) $[M]^+$, 105 (30). $C_{14}H_9N_3O_3S$ (299.30): calcd. C 56.18, H 3.03, N 14.04, S 10.71; found C 56.17, H 3.13, N 13.99, S 10.60.

5-(4-Nitrophenyl)-2-(pyrazin-2-yl)thiazol-4-ol (1b): A solution of pyrazine-2-carbothioamide (3.75 g, 26.9 mmol), ethyl 2-bromo-2-(4-nitrophenyl)acetate (9.30 g, 32.3 mmol, 1.2 equiv.), and pyridine (4.25 g, 53.8 mmol, 2 equiv.) in DMF (100 mL) was stirred at 50 °C for 24 h and a yellow precipitate was produced. After the system had cooled to room temperature, the mixture was diluted with EtOH (100 mL). The precipitate was filtered off, washed with EtOH and Et_2O, and dried in vacuo; yield 2.95 g (9.83 mmol, 37%). ^1H NMR (250 MHz, [D$_6$]DMSO): δ = 12.30 (s, J = 5.9 Hz, 1 H), 9.22 (s, 1 H), 8.73 (d, J = 13.4 Hz, 2 H), 8.25 (d, J = 7.9 Hz, 2 H), 8.04 (d, J = 8.9 Hz, 2 H) ppm. ^{13}C NMR (63 MHz, [D$_6$]-DMSO): δ = 160.91, 160.34, 145.64, 144.99, 144.85, 144.23, 139.75, 138.20, 126.29, 123.75, 109.40 ppm. UV/Vis (DMSO): λ_{max} [log(ε/M^{-1} cm^{-1})] = 419 [4.20] nm. MS (EI): m/z (%) = 300 (60) $[M]^+$, 106 (100). $C_{13}H_8N_4O_3S$ (300.29): calcd. C 52.00, H 2.69, N 18.66, S 10.68; found C 52.24, H 2.71, N 18.34, S 10.52.

5-(4-Nitrophenyl)-2-(pyrimidin-2-yl)thiazol-4-ol (1c): A mixture of pyrimidine-2-carbothioamide (2.60 g, 18.7 mmol), ethyl 2-bromo-2-(4-nitrophenyl)acetate (6.46 g, 22.4 mmol, 1.2 equiv.), and triethylamine (10 mL) was stirred at room temperature. The suspension solidified after a few minutes and was allowed to react for 24 h. The mixture was suspended in EtOH (100 mL). The precipitate was filtered off, washed with EtOH and Et_2O, and dried in vacuo; yield 1.12 g (3.73 mmol, 18%). ^1H NMR (400 MHz, [D$_6$]DMSO): δ = 12.34 (s, 1 H), 8.92 (d, J = 4.8 Hz, 2 H), 8.25 (d, J = 8.9 Hz, 2 H), 8.05 (d, J = 8.9 Hz, 2 H), 7.55 (t, J = 4.8 Hz, 1 H) ppm. ^{13}C NMR (100 MHz, [D$_6$]DMSO): δ = 161.28, 160.61, 157.97, 157.67, 144.85, 138.35, 126.32, 123.76, 121.20, 109.89 ppm. UV/Vis (DMSO): λ_{max} [log(ε/M^{-1} cm^{-1})] = 412 [4.10] nm. MS (EI): m/z (%) = 300 (60) $[M]^+$, 106 (100). $C_{13}H_8N_4O_3S$ (300.29): calcd. C 52.00, H 2.69, N 18.66, S 10.68; found C 51.64, H 2.81, N 18.54, S 10.72.

General procedure, illustrated for **2a**, for the etherification of the 4-hydroxy-1,3-thiazoles:

4-Methoxy-5-(4-nitrophenyl)-2-(pyridin-2-yl)thiazole (2a): A mixture of 5-(4-nitrophenyl)-2-(pyridin-2-yl)thiazol-4-ol (4.00 g, 13.4 mmol) and K_2CO_3 (2.22 g, 16.1 mmol, 1.2 equiv.) in DMSO

(100 mL) was stirred for 30 min, followed by the addition of CH_3I (2.09 g, 14.7 mmol, 1.1 equiv.). The deep blue mixture was stirred for 24 h at room temperature. The solution was poured into H_2O (300 mL) and extracted with $CHCl_3$ (3 × 100 mL). The combined organic phases were additionally washed with H_2O (3 × 100 mL) to remove the DMSO, dried with $MgSO_4$, and concentrated in vacuo to give a brown oil, which was further purified by a short gel filtration (silica, $CHCl_3$ to $CHCl_3$/EtOAc 1:1) to yield the product as an orange solid; yield 2.86 g (9.11 mmol, 68%). ^{1}H NMR (250 MHz, $CDCl_3$): δ = 8.61 (d, J = 4.2 Hz, 1 H), 8.26–8.18 (m, 2 H), 8.15 (d, J = 7.9 Hz, 1 H), 7.96–7.87 (m, 2 H), 7.81 (td, J = 7.7, 1.7 Hz, 1 H), 7.35 (ddd, J = 7.5, 4.8, 1.1 Hz, 1 H), 4.25 (s, 3 H) ppm. ^{13}C NMR (63 MHz, $CDCl_3$): δ = 163.44, 161.57, 150.65, 149.60, 145.46, 138.63, 137.03, 126.67, 124.85, 124.12, 119.31, 111.62, 57.89 ppm. UV/Vis (CH_2Cl_2): λ_{max} [log(ε/M^{-1} cm^{-1})] = 226 [4.05], 399 [4.49] nm. MS (EI): m/z (%) = 313 (100) [M]$^+$, 166 (45). $C_{15}H_{11}N_3O_3S$ (313.33): calcd. C 57.70, H 3.54, N 13.32, S 10.23; found C 57.70, H 3.86, N 13.32, S 10.19.

4-Methoxy-5-(4-nitrophenyl)-2-(pyrazin-2-yl)thiazole (2b): The procedure was similar to that used for **2a**, with purification by recrystallization from EtOH/$CHCl_3$ with slow evaporation of the $CHCl_3$ to give the product as yellow needles; yield 45%. ^{1}H NMR (250 MHz, $CDCl_3$): δ = 9.38 (d, J = 1.4 Hz, 1 H), 8.62 (d, J = 2.5 Hz, 1 H), 8.58–8.53 (m, 1 H), 8.28–8.19 (m, 2 H), 7.98–7.88 (m, 2 H), 4.28 (s, 3 H) ppm. ^{13}C NMR (63 MHz, $CDCl_3$): δ = 162.00, 160.55, 146.31, 145.97, 145.53, 144.14, 141.26, 138.22, 127.08, 124.32, 112.98, 58.27 ppm. UV/Vis (CH_3CN): λ_{max} [log(ε/M^{-1} cm^{-1})] = 245 [397], 403 [4.46] nm. MS (EI): m/z (%) = 314 (100) [M]$^+$, 166 (30). $C_{14}H_{10}N_4O_3S$ (314.32): calcd. C 53.50, H 3.21, N 17.82, S 10.20; found C 53.18, H 3.12, N 18.08, S 10.13.

4-Methoxy-5-(4-nitrophenyl)-2-(pyrimidin-2-yl)thiazole (2c): Yield 44%. ^{1}H NMR (300 MHz, $CDCl_3$): δ = 8.84 (d, J = 4.5 Hz, 2 H), 8.19 (d, J = 8.3 Hz, 2 H), 7.91 (d, J = 8.3 Hz, 2 H), 7.30 (t, J = 4.5 Hz, 1 H), 4.30 (s, 3 H) ppm. ^{13}C NMR (100 MHz, $CDCl_3$): δ = 162.16, 160.63, 158.91, 157.76, 145.79, 137.95, 127.00, 124.06, 120.78, 113.95, 58.29 ppm. UV/Vis (CH_3CN): λ_{max} [log(ε/M^{-1} cm^{-1})] = 232 [4.03], 396 [4.41] nm. MS (EI): m/z (%) = 314 (100) [M]$^+$, 166 (20). $C_{14}H_{10}N_4O_3S$ (314.32): calcd. C 53.50, H 3.21, N 17.82, S 10.20; found C 53.58, H 3.17, N 17.99, S 10.18.

5-(4-Bromophenyl)-4-methoxy-2-(pyridin-2-yl)thiazole (2d): Yield 77%. ^{1}H NMR (250 MHz, $CDCl_3$): δ = 9.15–9.10 (m, 1 H), 8.64 (d, J = 4.8 Hz, 1 H), 8.20–8.15 (m, 1 H), 7.61 (dd, J = 6.8 Hz, 2 H), 7.51 (dd, J = 6.8 Hz, 2 H), 7.39–7.34 (m, 1 H), 4.19 (s, 3 H) ppm. ^{13}C NMR (63 MHz, $CDCl_3$): δ = 160.01, 156.92, 150.67, 146.95, 132.63, 131.72, 130.21, 129.42, 128.26, 123.68, 120.43, 110.9, 57.96 ppm. MS (EI): m/z (%) = 346 (45) [M]$^+$, 200 (100), 120 (67). $C_{15}H_{11}BrN_2OS$ (347.23): calcd. C 51.89, H 3.19, N 8.07, S 9.23; found C 51.64, H 3.23, N 8.24, S 9.42.

General procedure, illustrated for **3a**, for the reduction of the nitro groups to afford the corresponding aniline derivatives:

4-[4-Methoxy-2-(pyridin-2-yl)thiazol-5-yl]aniline (3a): A suspension of 4-methoxy-5-(4-nitrophenyl)-2-(pyridin-2-yl)thiazole (2.66 g, 8.50 mmol) in EtOH (100 mL) was heated to 50 °C. Freshly prepared Raney nickel (catalytic amounts) and N_2H_5OH (several portions approx. 2 equiv. until no starting material was left as indicated by TLC) were added to the solution. The reaction mixture was filtered through a frit on which a silica bed (2 cm thick) had been applied to remove the Raney nickel. The silica bed was washed with EtOH/$CHCl_3$ 1:1. The product was purified by gradient gel filtration (silica, $CHCl_3$ to $CHCl_3$/EtOAc 1:2) to yield the amine as a yellow solid; yield 2.16 g (7.62 mmol, 90%). ^{1}H NMR (250 MHz, $CDCl_3$): δ = 3.76 (s, 2 H), 4.15 (s, 3 H), 6.68–6.72 (m, 2 H), 7.24 (dd, J = 4.8, 7.5 Hz, 1 H), 7.58–7.60 (m, 2 H), 7.74 (dd, J = 7.7, 7.8 Hz, 1 H), 8.10 (d, J = 8.0 Hz, 1 H), 8.57 (d, J = 4.9 Hz, 1 H) ppm. ^{13}C NMR (63 MHz, $CDCl_3$): δ = 158.63, 158.38, 151.51, 149.37, 145.53, 136.81, 128.28, 123.72, 121.91, 118.77, 115.42, 115.19, 57.58 ppm. UV/Vis (CH_2Cl_2): λ_{max} [log(ε/M^{-1} cm^{-1})] = 224 [4.01], 277 [3.83], 399 [4.19] nm. MS (EI): m/z (%) = 283 (100) [M]$^+$, 136 (60). $C_{15}H_{13}N_3OS$ (283.35): calcd. C 63.58, H 4.62, N 14.83, S 11.32; found C 63.20, H 4.57, N 14.60, S 11.19.

4-[4-Methoxy-2-(pyrazin-2-yl)thiazol-5-yl]aniline (3b): Yield 89%. ^{1}H NMR (300 MHz, $CDCl_3$): δ = 9.32 (d, J = 1.1 Hz, 1 H), 8.51–8.46 (m, 2 H), 7.58 (d, J = 8.6 Hz, 2 H), 6.70 (d, J = 8.6 Hz, 2 H), 4.17 (s, 3 H), 3.74 (s, 2 H) ppm. ^{13}C NMR (75 MHz, $CDCl_3$): δ = 159.20, 155.24, 147.11, 146.00, 144.16, 143.85, 140.96, 128.52, 121.51, 117.00, 115.25, 57.80 ppm. UV/Vis (CH_3CN): λ_{max} [log(ε/M^{-1} cm^{-1})] = 259 [4.02], 278 [3.98], 317 [3.68], 420 [4.31] nm. MS (EI): m/z (%) = 284 (100) [M]$^+$, 136 (80). $C_{14}H_{12}N_4OS$ (284.34): calcd. C 59.14, H 4.25, N 19.70, S 11.03; found C 58.84, H 4.18, N 19.52, S 11.08.

4-[4-Methoxy-2-(pyrimidin-2-yl)thiazol-5-yl]aniline (3c): Yield 87%. ^{1}H NMR (250 MHz, $CDCl_3$): δ = 8.79 (d, J = 4.9 Hz, 2 H), 7.60 (d, J = 8.6 Hz, 2 H), 7.20 (t, J = 4.8 Hz, 1 H), 6.69 (d, J = 8.6 Hz, 2 H), 4.22 (s, 3 H), 3.78 (s, 2 H) ppm. ^{13}C NMR (63 MHz, $CDCl_3$): δ = 159.84, 159.80, 157.84, 155.73, 146.13, 128.73, 128.67, 121.60, 119.97, 115.30, 58.10 ppm. UV/Vis (CH_3CN): λ_{max} [log(ε/M^{-1} cm^{-1})] = 223 [4.16], 243 [3.99], 275 [3.98], 411 [4.33] nm. MS (EI): m/z (%) = 284 (100) [M]$^+$, 136 (80). $C_{14}H_{12}N_4OS$ (284.34): calcd. C 59.14, H 4.25, N 19.70, S 11.03; found C 59.30, H 4.33, N 19.47, S 11.03.

General procedure, illustrated for **A1**, for the Buchwald–Hartwig couplings of the arylamines with the corresponding aryl halides:

4-[4-Methoxy-2-(pyridin-2-yl)thiazol-5-yl]-*N*,*N*-diphenylaniline (A1): Bromobenzene (345 mg, 2.2 mmol, 2.2 equiv.) and KO*t*Bu (246 mg, 2.2 mmol, 2.2 equiv.) were added under nitrogen to a solution of 4-[4-methoxy-2-(pyridin-2-yl)thiazol-5-yl]aniline (238 mg, 1 mmol) in dry toluene (20 mL). The mixture was additionally purged thoroughly with nitrogen for 30 min, followed by the addition of $Pd(dba)_2$ (23 mg, 0.04 mmol, 4 mol-%) and P(tBu)$_3$ (80 µL of a 1.0 M solution in toluene, 0.08 mmol, 8 mol-%). The mixture was heated to reflux (6 to 24 h) until no starting material was left as indicated by TLC (silica, $CHCl_3$, R_f starting material = 0.1, R_f monosubstituted product = 0.6, R_f disubstituted product = 0.8). After the reaction was complete, the mixture was allowed to cool down to room temp. and the solvent was evaporated in vacuo. Purification by column or flash chromatography yielded the product as a yellow solid. To obtain crystals suitable for X-ray crystallography, the product was recrystallized from EtOH/$CHCl_3$ to afford the compound as yellow block crystals; yield 331 mg (0.76 mmol, 76%). ^{1}H NMR (250 MHz, $CDCl_3$): δ = 8.59 (d, J = 4.3 Hz, 1 H), 8.12 (d, J = 7.9 Hz, 1 H), 7.77 (td, J = 7.7, 1.7 Hz, 1 H), 7.66 (d, J = 8.7 Hz, 2 H), 7.34–7.22 (m, 5 H), 7.19–6.95 (m, 8 H), 4.18 (s, 3 H) ppm. ^{13}C NMR (63 MHz, $CDCl_3$): δ = 159.23, 159.24, 151.36, 149.40, 147.47, 146.51, 136.82, 129.26, 127.74, 125.61, 124.51, 123.89, 123.51, 123.03, 118.86, 114.55, 57.58 ppm. UV/Vis ($CHCl_3$): λ_{max} [log(ε/M^{-1} cm^{-1})] = 306 [4.33], 417 [4.44] nm. MS (EI): m/z (%) = 435 (100) [M]$^+$, 288 (55). $C_{27}H_{21}N_3OS$ (435.54): calcd. C 74.46, H 4.86, N 9.65, S 7.36; found C 74.25, H 4.71, N 9.40, S 7.16.

Monosubstituted Product of A1. 4-[4-Methoxy-2-(pyridin-2-yl)thiazol-5-yl]-*N*-phenylaniline (A1m): If the reaction to **A1** was aborted earlier (t > 2 h), the monosubstituted product was obtained in 70% yield after purification (column chromatography, silica, $CHCl_3$). Recrystallization from EtOH/$CHCl_3$ yielded the compound as orange needles suitable for X-ray structure analysis. ^{1}H NMR

(250 MHz, $CDCl_3$): δ = 8.58 (d, J = 4.8 Hz, 1 H), 8.12 (d, J = 8.0 Hz, 1 H), 7.77 (td, J = 7.8, 1.7 Hz, 1 H), 7.69 (d, J = 8.7 Hz, 2 H), 7.36–7.22 (m, 3 H), 7.16–7.03 (m, 4 H), 6.96 (t, J = 7.3 Hz, 1 H), 5.79 (s, 1 H), 4.18 (s, 3 H) ppm. ^{13}C NMR (63 MHz, $CDCl_3$): δ = 158.99, 158.93, 151.45, 149.40, 142.58, 142.07, 136.82, 129.38, 128.11, 124.14, 123.82, 121.37, 118.84, 118.25, 117.45, 114.91, 57.60 ppm. UV/Vis (CH_3CN): λ_{max} [log(ε/M^{-1}cm^{-1})] = 229 [4.17], 295 [4.21], 405 [4.44] nm. MS (EI): m/z (%) = 359 (100) $[M]^+$, 212 (80). $C_{21}H_{17}N_3OS$ (359.44): calcd. C 70.17, H 4.77, N 11.69, S 8.92; found C 70.29, H 4.72, N 11.67, S 8.95.

4-Methoxy-*N*-{4-[4-methoxy-2-(pyridin-2-yl)thiazol-5-yl]phenyl}-*N*-(4-methoxyphenyl)aniline (A2): Yield 90%. ^{1}H NMR (400 MHz, $CDCl_3$): δ = 8.57 (d, J = 4.7 Hz, 1 H), 8.10 (d, J = 8.0 Hz, 1 H), 7.75 (td, J = 7.8, 1.7 Hz, 1 H), 7.63–7.56 (m, 2 H), 7.29–7.22 (m, 1 H), 7.11–7.03 (m, 4 H), 6.93 (d, J = 8.8 Hz, 2 H), 6.88–6.81 (m, 4 H), 4.15 (s, 3 H), 3.80 (s, 6 H) ppm. ^{13}C NMR (100 MHz, $CDCl_3$): δ = 159.17, 158.96, 156.21, 151.70, 149.56, 147.77, 140.89, 136.93, 127.85, 126.84, 123.90, 123.80, 120.61, 118.99, 115.31, 114.94, 57.70, 55.67 ppm. UV/Vis (CH_3CN): λ_{max} [log(ε/M^{-1}cm^{-1})] = 299 [4.35], 417 [4.43] nm. HRMS (ESI): calcd. 518.1514 $[C_{29}H_{25}N_3O_3S + Na]^+$; found 518.1517.

N^1-[4-(Dimethylamino)phenyl]-N^1-{4-[4-methoxy-2-(pyridin-2-yl)-thiazol-5-yl]phenyl}-N^4,N^4-dimethylbenzene-1,4-diamine (A3): Yield 86%. ^{1}H NMR (400 MHz, $CDCl_3$): δ = 8.56 (d, J = 4.5 Hz, 1 H), 8.10 (d, J = 7.9 Hz, 1 H), 7.74 (td, J = 7.8, 1.6 Hz, 1 H), 7.56 (d, J = 8.8 Hz, 2 H), 7.24 (dd, J = 7.0, 5.4 Hz, 1 H), 7.07 (d, J = 8.9 Hz, 4 H), 6.90 (d, J = 8.8 Hz, 2 H), 6.69 (d, J = 8.9 Hz, 4 H), 4.16 (s, 3 H), 2.93 (s, 12 H) ppm. ^{13}C NMR (100 MHz, $CDCl_3$): δ = 158.94, 158.39, 151.78, 149.52, 148.42, 147.63, 137.48, 136.88, 127.74, 127.03, 123.74, 122.34, 119.16, 118.91, 115.87, 113.81, 57.67, 41.10 ppm. UV/Vis (CH_3CN): λ_{max} [log(ε/M^{-1}cm^{-1})] = 247 [4.30], 206 [4.80], 307 [4.43], 433 [4.36] nm. MS (EI): m/z (%) = 521 (100) $[M]^+$, 374 (80). $C_{31}H_{31}N_5OS$: C 71.37, H 5.99, N 13.42, S 6.15; found C 71.23, H 4.66, N 13.17, S 5.77.

4-[4-Methoxy-2-(pyrazin-2-yl)thiazol-5-yl]-*N*,*N*-diphenylaniline (B1): Yield 90%. ^{1}H NMR (400 MHz, $CDCl_3$): δ = 9.34 (d, J = 1.3 Hz, 1 H), 8.53 (d, J = 2.5 Hz, 1 H), 8.52–8.49 (m, 1 H), 7.65 (d, J = 8.8 Hz, 2 H), 7.33–7.18 (m, 4 H), 7.17–7.00 (m, 8 H), 4.19 (s, 3 H) ppm. ^{13}C NMR (100 MHz, $CDCl_3$): δ = 159.72, 156.18, 147.42, 147.01, 146.92, 144.30, 143.77, 140.96, 129.33, 127.94, 125.01, 124.71, 123.26, 116.11, 109.95, 57.75 ppm. MS (EI): m/z (%) = 436 (100) $[M]^+$, 288 (90). UV/Vis (CH_3CN): λ_{max} [log(ε/M^{-1}cm^{-1})] = 237 [4.01], 303 [4.20], 426 [4.27] nm. $C_{26}H_{20}N_4OS$ (436.53): calcd. C 71.54, H 4.62, N 12.83, S 7.35; found C 71.27, H 4.66, N 12.61, S 7.67.

Monosubstituted Product of B1 – 4-[4-Methoxy-2-(pyrazin-2-yl)thiazol-5-yl]-*N*-phenylaniline (B1m): If the reaction to afford **B1** was aborted earlier (t > 3 h), the monosubstituted product was obtained in 79% yield after purification (column chromatography, silica, $CHCl_3$/EtOAc 4:1). Recrystallization from EtOH/$CHCl_3$ yielded the compound as orange block crystals. ^{1}H NMR (250 MHz, $CDCl_3$): δ = 8.82 (d, J = 4.9 Hz, 2 H), 7.76–7.68 (m, 2 H), 7.33–7.20 (m, 3 H), 7.17–7.04 (m, 4 H), 7.02–6.91 (m, 1 H), 5.88 (s, 1 H), 4.26 (s, 3 H) ppm. ^{13}C NMR (63 MHz, $CDCl_3$): δ = 160.10, 159.70, 157.83, 156.20, 142.81, 142.44, 129.54, 128.54, 123.57, 121.75, 120.06, 118.65, 117.89, 117.29, 58.11 ppm. MS (EI): m/z (%) = 360 (50) $[M]^+$, 212 (100). $C_{20}H_{16}N_4OS$ (360.43): calcd. C 66.65, H 4.47, N 15.54, S 8.90; found C 66.60, H 4.45, N 15.60, S 8.79.

4-Methoxy-*N*-{4-[4-methoxy-2-(pyrazin-2-yl)thiazol-5-yl]phenyl}-*N*-(4-methoxyphenyl)aniline (B2): Yield 84%. ^{1}H NMR (400 MHz, $CDCl_3$): δ = 9.33 (d, J = 1.4 Hz, 1 H), 8.51 (d, J = 2.5 Hz, 1 H), 8.50–8.48 (m, 1 H), 7.61–7.55 (m, 2 H), 7.10–7.04 (m, 4 H), 6.95–6.90 (m, 2 H), 6.87–6.81 (m, 4 H), 4.17 (s, 3 H), 3.80 (s, 6 H) ppm. ^{13}C NMR (100 MHz, $CDCl_3$): δ = 159.56, 156.25, 155.61, 148.09, 147.11, 144.26, 143.91, 141.04, 140.63, 127.95, 126.94, 123.04, 120.26, 116.70, 114.90, 57.86, 55.64 ppm. UV/Vis (CH_3CN): λ_{max} [log(ε/M^{-1}cm^{-1})] = 240 [4.42], 302 [4.40], 439 [4.46] nm. MS (micro-ESI): m/z = 519.1 $[M + Na]^+$. $C_{28}H_{24}N_4O_3S$ (496.58): calcd. C 67.72, H 4.87, N 11.28, S 6.46; found C 67.39, H 4.88, N 11.16, S 6.15.

4-[4-Methoxy-2-(pyrimidin-2-yl)thiazol-5-yl]-*N*,*N*-di-*p*-tolylaniline (C1): Yield 85%. ^{1}H NMR (400 MHz, $CDCl_3$): δ = 8.83 (d, J = 4.9 Hz, 1 H), 7.65 (d, J = 8.8 Hz, 1 H), 7.24 (t, J = 4.9 Hz, 1 H), 7.13–7.07 (m, 2 H), 7.07–7.00 (m, 3 H), 4.26 (s, 2 H), 2.34 (s, 3 H) ppm. ^{13}C NMR (100 MHz, $CDCl_3$): δ = 160.23, 159.71, 157.85, 156.29, 147.69, 145.01, 133.13, 130.10, 128.08, 125.10, 124.04, 122.10, 120.06, 117.89, 58.11, 20.98 ppm. UV/Vis (CH_3CN): λ_{max} [log(ε/M^{-1}cm^{-1})] = 233 [4.21], 302 [4.32], 426 [4.36] nm. MS (EI): m/z (%) = 464 (30) $[M]^+$, 316 (100). HRMS (micro-ESI): $C_{28}H_{24}N_4OS$: 464.1671; found 464.1665. $C_{28}H_{24}N_4OS$ (464.58): calcd. C 72.39, H 5.21, N 12.06, S 6.90; found C 72.30, H 5.33, N 12.47, S 6.03.

4-Methoxy-*N*-{4-[4-methoxy-2-(pyrimidin-2-yl)thiazol-5-yl]phenyl}-*N*-(4-methoxyphenyl)aniline (C2): Yield 90%. ^{1}H NMR (250 MHz, $CDCl_3$): δ = 8.80 (d, J = 4.9 Hz, 2 H), 7.61 (d, J = 8.8 Hz, 2 H), 7.25–7.17 (m, 1 H), 7.13–7.03 (m, 4 H), 6.93 (d, J = 8.8 Hz, 2 H), 6.88–6.79 (m, 4 H), 4.23 (s, 3 H), 3.80 (s, 6 H) ppm. ^{13}C NMR (63 MHz, $CDCl_3$): δ = 160.09, 159.71, 157.82, 156.25, 155.99, 148.20, 140.60, 128.07, 126.95, 122.99, 120.21, 119.99, 118.08, 114.89, 58.08, 55.62 ppm. UV/Vis (CH_3CN): λ_{max} [log(ε/M^{-1}cm^{-1})] = 231 [4.36], 301 [4.38], 433 [4.46] nm. MS (EI): m/z (%) = 496 (100) $[M]^+$, 348 (90). HRMS (micro-ESI): $C_{28}H_{24}N_4O_3S$: 496.1569; found 496.1568. $C_{28}H_{24}N_4O_3S$: C 67.72, H 4.87, N 11.28, S 6.46; found C 67.69, H 4.83, N 11.46, S 6.03.

5-[4-(9*H*-Carbazol-9-yl)phenyl]-4-methoxy-2-(pyridin-2-yl)thiazole (D1): The procedure was similar to that used for **A1**. Instead of P(tBu)$_3$, SPHOS was used as the phosphane ligand. Compound **2d** (393 mg, 1.13 mmol), $Pd(dba)_2$ (13 mg, 0.023 mmol, 2 mol-%), SPOS (18 mg, 0.046 mmol, 4 mol-%), carbazole (208 mg, 1.25 mmol, 1.1 equiv.), KOtBu (140 mg, 1.25 mmol, 1.1 equiv.), and toluene (dry and degassed, 30 mL) were used. Purification was by column chromatography (silica, $CHCl_3$/EtOAc 10:1, R_f starting material = 0.7, R_f product = 0.75!) and additionally by recrystallization from EtOH/$CHCl_3$ by slow evaporation of the $CHCl_3$, to yield the arylamine as a yellow amorphous solid; yield 336 mg (0.78 mmol), 69%. ^{1}H NMR (400 MHz, $CDCl_3$): δ = 8.63 (d, J = 4.7 Hz, 1 H), 8.22–8.12 (m, 3 H), 8.03 (d, J = 8.5 Hz, 2 H), 7.81 (td, J = 7.7, 1.4 Hz, 1 H), 7.60 (d, J = 8.5 Hz, 2 H), 7.53–7.38 (m, 4 H), 7.37–7.23 (m, 3 H), 4.27 (s, 3 H) ppm. ^{13}C NMR (100 MHz, $CDCl_3$): δ = 161.13, 160.25, 151.39, 149.67, 141.00, 137.06, 136.19, 131.12, 128.36, 127.38, 126.12, 124.41, 123.63, 120.44, 120.15, 119.22, 113.59, 110.03, 57.87 ppm. UV/Vis ($CHCl_3$): λ_{max} [log(ε/M^{-1}cm^{-1})] = 293 [4.04], 387 [4.13] nm. UV/Vis (CH_3CN): λ_{max} [log(ε/M^{-1}cm^{-1})] = 236 [4.49], 292 [4.11], 380 [4.24] nm. MS (EI): m/z (%) = 433 (100) $[M]^+$, 286 (90). $C_{27}H_{19}N_3OS$ (433.53): calcd. C 74.80, H 4.42, N 9.69, S 7.40; found C 74.79, H 4.30, N 9.39, S 7.26.

10-{4-[4-Methoxy-2-(pyridin-2-yl)thiazol-5-yl]phenyl}-10*H*-phenothiazine (D2): The procedure was similar to that used for **D1**; yield 88%. Purification was achieved by recrystallization from $CHCl_3$. ^{1}H NMR (400 MHz, $CDCl_3$): δ = 8.62 (ddd, J = 4.8, 1.5, 0.8 Hz, 1 H), 8.16 (d, J = 7.9 Hz, 1 H), 8.03–7.97 (m, 2 H), 7.80 (td, J = 7.8, 1.7 Hz, 1 H), 7.42–7.36 (m, 2 H), 7.32 (ddd, J = 7.5, 4.8, 1.1 Hz, 1

H), 7.04 (dd, J = 7.4, 1.7 Hz, 2 H), 6.92–6.78 (m, 4 H), 6.34 (dd, J = 8.1, 1.2 Hz, 2 H), 4.24 (s, 3 H) ppm. ^{13}C NMR (100 MHz, $CDCl_3$): δ = 161.20, 160.27, 151.30, 149.68, 144.28, 139.55, 137.10, 131.66, 130.74, 129.08, 127.03, 126.94, 124.48, 122.77, 120.85, 119.24, 116.66, 113.38, 57.88 ppm. UV/Vis (THF): λ_{max} [log(ε/M^{-1} cm^{-1})] = 257 [4.72], 377 [4.42] nm. MS (EI): m/z (%) = 465 (100) [M]$^+$, 318 (90). $C_{27}H_{19}N_3OS_2$ (465.59): calcd. C 69.65, H 4.11, N 9.03, S 13.77; found C 69.55, H 4.02, N 9.21, S 13.89.

10-{4-[4-Methoxy-2-(pyridin-2-yl)thiazol-5-yl]phenyl}-10*H*-phenoxazine (D3): Yield 80%. ^{1}H NMR (400 MHz, $CDCl_3$): δ = 8.62 (ddd, J = 4.8, 1.5, 0.9 Hz, 1 H), 8.16 (d, J = 7.9 Hz, 1 H), 8.03–7.97 (m, 2 H), 7.80 (td, J = 7.8, 1.7 Hz, 1 H), 7.39–7.29 (m, 3 H), 6.72–6.57 (m, 6 H), 6.02 (dd, J = 7.7, 1.6 Hz, 2 H), 4.24 (s, 3 H) ppm. ^{13}C NMR (100 MHz, $CDCl_3$): δ = 161.32, 160.32, 151.26, 149.67, 144.11, 137.24, 137.11, 134.47, 132.20, 131.21, 129.40, 124.51, 123.40, 121.46, 119.25, 115.56, 113.49, 113.24 57.88 ppm. UV/Vis (CH_3CN): λ_{max} [log(ε/M^{-1} cm^{-1})] = 240 [4.77], 276 [4.06], 373 [4.40] nm. MS (EI): m/z (%) = 449 (50) [M]$^+$, 302 (100). $C_{27}H_{19}N_3O_2S$ (449.53): calcd. C 72.14, H 4.26, N 9.35, S 7.13; found C 72.09, H 4.12, N 9.44, S 7.55.

General Procedure, illustrated for **Ru1**, for the synthesis of the Ru(dmbpy)$_2$(L)(PF$_6$)$_2$ complexes:

Ru(dmbpy)$_2$(*A1*)(PF$_6$)$_2$ (Ru1): The activated precursor *cis*-Ru(dmbpy)$_2$(acetone)$_2$(PF$_6$)$_2$ was synthesized by stirring *cis*-(dmbpy)$_2$RuCl$_2$ (68 mg, 0.126 mmol) and AgPF$_6$ (64 mg, 0.252 mmol, 2 equiv.) in dried and nitrogen-purged acetone (5 mL) for 6 h at room temp. under inert conditions with use of Schlenk techniques. The precipitated AgCl was filtered off and the corresponding ligand **A1** (55 mg, 0.126 mmol) was added to the solution. The mixture was heated under reflux for 24 h. Subsequently, the reaction mixture was allowed to cool to room temp. and filtered through a cellulose filter. The solvent was removed in vacuo and the crude product was purified by size exclusion chromatography (Bio-Beads S-X1, CH_2Cl_2 as eluent) to remove traces of the ligand (if the complex was not sufficiently soluble in CH_2Cl_2, it was applied with a 1:1 mixture of CH_2Cl_2/acetone and eluted with CH_2Cl_2). After evaporation of the solvent, the solid was dissolved in a small amount of CH_2Cl_2 and precipitated with Et_2O (200 mL) to give the complex as a red solid; yield 99 mg (0.083 mmol, 67%). ^{1}H NMR (250 MHz, CD_3CN): δ = 8.39–8.26 (m, 4 H), 8.20 (d, J = 7.9 Hz, 1 H), 7.97 (td, J = 7.9, 1.2 Hz, 1 H), 7.91 (d, J = 5.8 Hz, 1 H), 7.63 (d, J = 5.5 Hz, 1 H), 7.59 (d, J = 5.8 Hz, 2 H), 7.50–6.88 (m, 20 H), 2.99 (s, 3 H), 2.61–2.46 (m, 12 H) ppm. ^{13}C NMR (63 MHz, CD_3CN): δ = 161.39, 158.02, 157.99, 157.94, 157.51, 157.50, 154.59, 152.79, 152.23, 152.01, 151.61, 151.31, 151.23, 151.21, 150.64, 150.22, 147.70, 138.52, 130.66, 129.67, 129.41, 129.29, 129.19, 128.30, 127.85, 126.46, 125.88, 125.83, 125.49, 125.46, 125.42, 124.99, 124.18, 122.23, 121.17, 62.11, 21.24, 21.18, 21.11 ppm. UV/Vis (CH_3CN): λ_{max} [log(ε/M^{-1} cm^{-1})] = 258 [4.47], 287 [492], 319 [4.59], 447 [4.48] nm. MS (MALDI-TOF, dithranol): calcd. for $C_{51}H_{45}F_6N_7OPRuS$ 1050.209 [M – PF$_6$]$^+$; found 1050.345. HRMS (micro-ESI): calcd. for $C_{51}H_{45}F_6N_7OPRuS$ 1044.2124; found 1044.2122.

Ru(dmbpy)$_2$(*A2*)(PF$_6$)$_2$ (Ru2): Yield 67%. ^{1}H NMR (400 MHz, CD_3CN): δ = 8.36–8.31 (m, 3 H), 8.28 (s, 1 H), 8.17 (d, J = 8.0 Hz, 1 H), 7.96 (td, J = 7.9, 1.3 Hz, 1 H), 7.90 (d, J = 5.8 Hz, 1 H), 7.62 (d, J = 5.6 Hz, 1 H), 7.58 (d, J = 5.8 Hz, 2 H), 7.45 (d, J = 5.8 Hz, 1 H), 7.36–7.25 (m, 5 H), 7.21 (d, J = 5.8 Hz, 1 H), 7.16 (d, J = 5.8 Hz, 1 H), 7.13–7.07 (m, 4 H), 6.96–6.90 (m, 4 H), 6.80 (d, J = 8.9 Hz, 2 H), 3.78 (s, 6 H), 2.98 (s, 3 H), 2.56 (s, 3 H), 2.55 (s, 3 H), 2.53 (s, 3 H), 2.50 (s, 3 H) ppm. ^{13}C NMR (100 MHz, CD_3CN): δ = 161.20, 158.30, 158.16, 158.13, 158.10, 157.66, 157.01, 154.80, 152.88, 152.85, 152.32, 152.12, 151.72, 151.43, 151.42, 151.35, 151.33, 150.75, 140.43, 138.61, 129.63, 129.51, 129.40, 129.29, 128.93, 128.40, 127.81, 126.13, 125.98, 125.94, 125.59, 125.10, 124.15, 119.03, 118.90, 116.11, 62.10, 56.25, 21.35, 21.34, 21.28, 21.21 ppm. UV/Vis (CH_3CN): λ_{max} [log(ε/M^{-1} cm^{-1})] = 248 [445], 258 [4.41], 286 [4.86], 324 [4.52], 457 [4.45] nm. MS (MALDI-TOF, dithranol): calcd. for $C_{53}H_{49}F_6N_7O_3PRuS$ 1110.26 [M – PF$_6$]$^+$; found 1110.23. HRMS (micro-ESI): calcd. for $C_{53}H_{49}F_6N_7O_3PRuS$ 1104.2335; found 1104.2336.

Ru(dmbpy)$_2$(*C1*)(PF$_6$)$_2$ (Ru3): Yield 60%. ^{1}H NMR (400 MHz, CD_3CN): δ = 8.84 (dd, J = 4.8, 1.9 Hz, 1 H), 8.37–8.29 (m, 4 H), 7.93 (d, J = 5.8 Hz, 1 H), 7.86 (dd, J = 5.8, 1.9 Hz, 1 H), 7.75 (d, J = 5.8 Hz, 1 H), 7.57 (d, J = 5.8 Hz, 1 H), 7.44 (d, J = 5.8 Hz, 1 H), 7.41 (d, J = 8.9 Hz, 2 H), 7.37–7.33 (m, 1 H), 7.33–7.28 (m, 2 H), 7.22 (d, J = 4.9 Hz, 1 H), 7.19–7.13 (m, 5 H), 7.01 (d, J = 8.3 Hz, 4 H), 6.89 (d, J = 8.9 Hz, 2 H), 3.00 (s, 3 H), 2.56 (d, J = 2.6 Hz, 6 H), 2.51 (d, J = 6.2 Hz, 6 H), 2.31 (s, 6 H) ppm. ^{13}C NMR (100 MHz, CD_3CN): δ = 164.05, 161.96, 160.34, 158.28, 158.09, 158.04, 157.86, 157.48, 155.41, 153.13, 152.72, 152.08, 151.89, 151.63, 151.59, 151.54, 150.96, 150.93, 145.00, 135.65, 131.29, 129.71, 129.66, 129.39, 129.36, 129.28, 128.45, 126.89, 126.01, 125.94, 125.61, 125.14, 122.84, 120.65, 120.04, 62.20, 21.31, 21.24, 21.18, 20.93 ppm. UV/Vis (CH_3CN): λ_{max} [log(ε/M^{-1} cm^{-1})] = 247 [4.58], 258 [4.54], 285 [4.99], 326 [4.64], 471 [4.53] nm. MS (MALDI-TOF, dithranol): calcd. for $C_{52}H_{48}F_6N_8OPRuS$ 1079.2718 [M – PF$_6$]$^+$; found 1079.2713. HRMS (micro-ESI): calcd. for $C_{52}H_{48}F_6N_8OPRuS$ 1073.2389; found 1073.2400.

Ru(dmbpy)$_2$(*C2*)(PF$_6$)$_2$ (Ru4): Yield 75%. ^{1}H NMR (400 MHz, CD_3CN): δ = 8.83 (dd, J = 4.8, 1.9 Hz, 1 H), 8.34 (s, 2 H), 8.31 (d, J = 8.6 Hz, 2 H), 7.92 (d, J = 5.8 Hz, 1 H), 7.85 (dd, J = 5.8, 1.9 Hz, 1 H), 7.75 (d, J = 5.8 Hz, 1 H), 7.57 (d, J = 5.8 Hz, 1 H), 7.43 (d, J = 5.8 Hz, 1 H), 7.40–7.35 (m, 2 H), 7.35–7.26 (m, 3 H), 7.21 (d, J = 5.8 Hz, 1 H), 7.17 (d, J = 5.8 Hz, 1 H), 7.14–7.07 (m, 4 H), 6.95–6.89 (m, 4 H), 6.82–6.75 (m, 2 H), 3.78 (s, 6 H), 2.98 (s, J = 6.0 Hz, 3 H), 2.56 (s, 3 H), 2.55 (s, 3 H), 2.52 (s, 3 H), 2.50 (s, 3 H) ppm. ^{13}C NMR (100 MHz, CD_3CN): δ = 164.07, 161.79, 160.32, 158.30, 158.27, 158.09, 158.04, 157.87, 157.48, 155.02, 153.12, 152.72, 152.08, 151.89, 151.61, 151.58, 151.53, 150.96, 140.21, 129.72, 129.65, 129.38, 129.27, 128.97, 128.44, 126.01, 125.94, 125.61, 125.14, 122.75, 118.86, 118.61, 116.05, 62.13, 56.19, 21.31, 21.24, 21.18 ppm. UV/Vis (CH_3CN): λ_{max} [log(ε/M^{-1} cm^{-1})] = 247 [4.62], 258 [4.57], 285 [5.00], 328 [4.63], 473 [4.55] nm. MS (MALDI-TOF, dithranol): calcd. for $C_{52}H_{48}F_6N_8O_3PRuS$ 1111.23 [M – PF$_6$]$^+$; found 1111.30. HRMS (micro-ESI): calcd. for $C_{52}H_{48}F_6N_8O_3PRuS$ 1105.2288; found 1105.2274.

Ru(dmbpy)$_2$(*D1*)(PF$_6$)$_2$ (Ru5): Yield 93%. ^{1}H NMR (400 MHz, CH_3CN): δ = 8.41–8.25 (m, 5 H), 8.20 (d, J = 7.8 Hz, 2 H), 8.02 (dd, J = 11.3, 4.4 Hz, 1 H), 7.98 (d, J = 5.8 Hz, 1 H), 7.83 (d, J = 8.6 Hz, 2 H), 7.74 (d, J = 8.5 Hz, 2 H), 7.69 (d, J = 5.5 Hz, 1 H), 7.63 (d, J = 5.8 Hz, 2 H), 7.51–7.41 (m, 5 H), 7.40–7.28 (m, 5 H), 7.24 (d, J = 5.1 Hz, 1 H), 7.19 (d, J = 5.0 Hz, 1 H), 3.09 (s, 3 H), 2.58 (s, 3 H), 2.57 (s, 3 H), 2.54 (s, 3 H), 2.52 (s, 3 H) ppm. ^{13}C NMR (100 MHz, CH_3CN): δ = 162.46, 159.40, 158.15, 158.10, 158.08, 157.62, 154.58, 152.98, 152.94, 152.33, 152.11, 151.70, 151.45, 151.39, 151.37, 150.80, 141.41, 139.72, 138.67, 130.67, 129.50, 129.37, 129.30, 128.53, 128.40, 128.30, 127.91, 127.31, 125.97, 125.94, 125.61, 125.11, 124.64, 124.54, 123.88, 121.55, 121.45, 110.72, 62.63, 21.31, 21.30, 21.24, 21.17 ppm. UV/Vis (CH_3CN): λ_{max} [log(ε/M^{-1} cm^{-1})] = 238 [4.73], 257 [4.53], 286 [4.85], 322 [4.38], 338 [4.34], 389 [4.29], 486 [4.00] nm. MS (MALDI-TOF, dithranol): calcd. for $C_{51}H_{43}F_6N_7OPRuS$ 1110.26 [M – PF$_6$]$^+$; found 1110.23. HRMS (micro-ESI): calcd. for $C_{51}H_{43}F_6N_7OPRuS$ 1042.1968; found 1042.1959.

Ru(dmbpy)$_2$(*D2*)(PF$_6$)$_2$ (Ru6): Yield 57%. ^{1}H NMR (400 MHz, CD_3CN): δ = 8.36 (s, 2 H), 8.35 (s, 1 H), 8.31 (s, 1 H), 8.26 (d, J = 7.9 Hz, 1 H), 8.01 (td, J = 7.9, 1.3 Hz, 1 H), 7.95 (d, J = 5.8 Hz, 1 H), 7.69–7.64 (m, 3 H), 7.63–7.59 (m, 2 H), 7.47 (d, J = 5.8 Hz, 1 H), 7.38–7.32 (m, 4 H), 7.30 (d, J = 4.9 Hz, 1 H), 7.27 (dd, J = 7.6, 1.5 Hz, 2 H), 7.24 (d, J = 5.8 Hz, 1 H), 7.18 (d, J = 4.8 Hz, 1 H), 7.13 (td, J = 7.8, 1.6 Hz, 2 H), 7.05 (td, J = 7.5, 1.3 Hz, 2 H), 6.73 (dd, J = 8.0, 1.0 Hz, 2 H), 3.03 (s, 3 H), 2.58 (s, 3 H), 2.57 (s, 3 H), 2.54 (s, 3 H), 2.52 (s, 3 H) ppm. ^{13}C NMR (100 MHz, CD_3CN): δ = 162.05, 158.80, 158.09, 158.06, 158.03, 157.58, 154.58, 152.93, 152.91, 152.32, 152.09, 151.70, 151.41, 151.34, 151.31, 150.75, 145.18, 143.78, 138.63, 130.92, 129.47, 129.36, 129.26, 128.62, 128.42, 128.37, 128.17, 126.71, 126.34, 125.95, 125.91, 125.59, 125.44, 125.08, 124.52, 124.36, 121.66, 21.33, 21.31, 21.26, 21.18, 15.64 ppm. UV/Vis (CH_3CN): λ_{max} [log(ε/M^{-1} cm^{-1})] = 257 [4.76], 286 [4.82], 320 [4.38], 367 [4.27], 434 [4.24] nm. MS (MALDI-TOF, dithranol): calcd. for $C_{51}H_{43}F_6N_7OPRuS_2$ 1080.17 [M – PF$_6$]$^+$; found 1080.17. HRMS (micro-ESI): calcd. for $C_{51}H_{43}F_6N_7OPRuS_2$ 1074.1692; found 1074.1711. $C_{51}H_{43}F_{12}N_7OP_2RuS_2$ (1225.06): calcd. C 50.00, H 3.54, N 8.00, S 5.23; found C 49.98, H 3.76, N 7.87, S 4.87.

Ru(dmbpy)$_2$(*D3*)(PF$_6$)$_2$ (Ru7): Yield 68%. ^{1}H NMR (400 MHz, CD_3CN): δ = 8.42–8.28 (m, 5 H), 8.04 (td, J = 7.9, 1.3 Hz, 1 H), 7.98 (d, J = 5.8 Hz, 1 H), 7.88–7.79 (m, 2 H), 7.70 (d, J = 5.3 Hz, 1 H), 7.63 (d, J = 5.8 Hz, 2 H), 7.54–7.47 (m, 3 H), 7.44–7.35 (m, 2 H), 7.32 (dd, J = 5.7, 0.9 Hz, 1 H), 7.25 (dd, J = 5.8, 0.9 Hz, 1 H), 7.20 (dd, J = 5.8, 0.9 Hz, 1 H), 6.73–6.60 (m, 6 H), 5.98 (d, J = 8.4 Hz, 2 H), 3.07 (d, J = 6.1 Hz, 3 H), 2.59 (s, 3 H), 2.59 (s, 3 H), 2.56 (s, 3 H), 2.54 (s, 3 H) ppm. ^{13}C NMR (100 MHz, CD_3CN): δ = 162.51, 159.65, 158.11, 158.06, 158.03, 157.58, 154.51, 153.00, 152.95, 152.33, 152.11, 151.71, 151.44, 151.37, 151.35, 150.78, 144.78, 141.24, 138.66, 134.93, 132.76, 131.88, 129.49, 129.37, 129.36, 129.29, 128.40, 128.36, 125.97, 125.93, 125.60, 125.09, 124.70, 124.56, 123.57, 122.82, 116.44, 114.40, 62.64, 21.32, 21.26, 21.18 ppm. UV/Vis (CH_3CN): λ_{max} [log(ε/M^{-1} cm^{-1})] = 286 [4.82], 327 [4.47], 446 [4.12], 483 [4.05] nm. MS (MALDI-TOF, dithranol): calcd. for $C_{51}H_{43}F_6N_7O_2PRuS$ 1064.19 [M – PF$_6$]$^+$; found 1064.20. HRMS (micro-ESI): calcd. for $C_{51}H_{43}F_6N_7O_2PRuS$: 1058.1916; found 1058.1923.

Supporting Information (see footnote on the first page of this article): Lippert–Mataga calculation, emission spectra of the dyes and of **A2** and **D1** in different solvents, ^{1}H NMR spectra of the radical cations of **A3** and **Ru4**, X-ray structure of **A1m**, refinement data and X-ray structure files for **A1**, **B1**, **C1**, **D2** and **A1m**, MALDI-TOF spectra of the complexes, graphical representation of the torsion angles for **A2** and **D1**, summary of the photophysical properties and representations of the orbitals of the higher excited singlet states, CV spectra of the complexes **Ru3**, **Ru4** and **Ru7**. ^{1}H and ^{13}C NMR spectra of the final products.

Acknowledgments

The authors thank the Thuringian Ministry for Education, Science and Culture (grant number #B514–09049, project "Photonische Mizellen [PhotoMIC]") for financial support. We gratefully acknowledge the help of Dr. Eckhard Birckner and Erika Kielman with the emission spectroscopy of the complexes at 77 K.

[1] R. M. Dodson, H. W. Turner, *J. Am. Chem. Soc.* **1951**, *73*, 4517–4519.

[2] J. Liebscher, *Houben–Weyl Methoden der Organischen Chemie*, vol. E8b, 4th ed., Thieme, Stuttgart, Germany, **1994**.

[3] a) F. A. J. Kerdesky, C. D. W. Brooks, K. I. Hulkower, J. B. Bouska, R. L. Bell, *Bioorg. Med. Chem.* **1997**, *5*, 393–396; b) R. M. Rzasa, M. R. Kaller, G. Liu, E. Magal, T. T. Nguyen, T. D. Osslund, D. Powers, V. J. Santora, V. N. Viswanadhan, H.-L. Wang, X. Xiong, W. Zhong, M. H. Norman, *Bioorg. Med. Chem.* **2007**, *15*, 6574–6595; c) F. A. J. Kerdesky, J. H. Holms, J. L. Moore, R. L. Bell, R. D. Dyer, G. W. Carter, D. W. Brooks, *J. Med. Chem.* **1991**, *34*, 2158–2165.

[4] R. Menzel, A. Breul, C. Pietsch, J. Schäfer, C. Friebe, E. Täuscher, D. Weiß, B. Dietzek, J. Popp, R. Beckert, U. S. Schubert, *Macromol. Chem. Phys.* **2011**, *212*, 840–848.

[5] B. Happ, J. Schafer, R. Menzel, M. D. Hager, A. Winter, J. Popp, R. Beckert, B. Dietzek, U. S. Schubert, *Macromolecules (Washington, DC, USA)* **2011**, *44*, 6277–6287.

[6] R. Menzel, D. Ogermann, S. Kupfer, D. Weiß, H. Görls, K. Kleinermanns, L. González, R. Beckert, *Dyes Pigm.* **2012**, *94*, 512–524.

[7] L. K. Calderón-Ortiz, E. Täuscher, E. Leite Bastos, H. Görls, D. Weiß, R. Beckert, *Eur. J. Org. Chem.* **2012**, 2535–2541.

[8] R. Menzel, E. Täuscher, D. Weiß, R. Beckert, H. Görls, *Z. Anorg. Allg. Chem.* **2010**, *636*, 1380–1385.

[9] a) S. Campagna, F. Puntoriero, F. Nastasi, G. Bergamini, V. Balzani, in: *Photochemistry and Photophysics of Coordination Compounds I*, vol. 280 (Eds.: V. Balzani, S. Campagna), Springer, Berlin, **2007**, pp. 117–214; b) V. Balzani, G. Bergamini, S. Campagna, F. Puntoriero, vol. 280 (Eds.: V. Balzani, S. Campagna), Springer Berlin/Heidelberg, **2007**, pp. 1–36; c) V. Balzani, A. Juris, *Coord. Chem. Rev.* **2001**, *211*, 97–115; d) J. P. Collin, S. Guillerez, J. P. Sauvage, F. Barigelletti, L. De Cola, L. Flamigni, V. Balzani, *Inorg. Chem.* **1991**, *30*, 4230–4238; e) V. Balzani, A. Juris, M. Venturi, S. Campagna, S. Serroni, *Chem. Rev.* **1996**, *96*, 759–834.

[10] a) G. J. Meyer, *Inorg. Chem.* **2005**, *44*, 6852–6864; b) N. L. Fry, P. K. Mascharak, *Acc. Chem. Res.* **2011**, *44*, 289–298; c) M. Su, W. Wei, S. Liu, *Anal. Chim. Acta* **2011**, *704*, 16–32; d) D. B. Watson, *Ruthenium: Properties, Production and Applications*, 1st ed., Nova Science Publishers Inc, New York, **2011**, pp. 157–188; e) G. C. Vougioukalakis, R. H. Grubbs, *Chem. Rev.* **2009**, *110*, 1746–1787; f) G. C. Vougioukalakis, A. I. Philippopoulos, T. Stergiopoulos, P. Falaras, *Coord. Chem. Rev.* **2011**, *255*, 2602–2621.

[11] M. Thelakkat, C. Schmitz, C. Hohle, P. Strohriegl, H.-W. Schmidt, U. Hofmann, S. Schloter, D. Haarer, *Phys. Chem. Chem. Phys.* **1999**, *1*, 1693–1698.

[12] X. Ma, F. Ma, Z. Zhao, N. Song, J. Zhang, *J. Mater. Chem.* **2010**, *20*, 2369–2380.

[13] a) M. Thelakkat, *Macromol. Mater. Eng.* **2002**, *287*, 442–461; b) C.-H. Yang, F.-J. Liu, L.-R. Huang, T.-L. Wang, W.-C. Lin, M. Sato, C.-H. Chen, C.-C. Chang, *J. Electroanal. Chem.* **2008**, *617*, 101–110; c) Z. Jiang, T. Ye, C. Yang, D. Yang, M. Zhu, C. Zhong, J. Qin, D. Ma, *Chem. Mater.* **2011**, *23*, 771–777.

[14] a) G. Wei, X. Xiao, S. Wang, J. D. Zimmerman, K. Sun, V. V. Diev, M. E. Thompson, S. R. Forrest, *Nano Lett.* **2011**, *11*, 4261–4264; b) W. Zhang, S. C. Tse, J. Lu, Y. Tao, M. S. Wong, *J. Mater. Chem.* **2010**, *20*, 2182–2189; c) L. Zhang, C. He, J. Chen, P. Yuan, L. Huang, C. Zhang, W. Cai, Z. Liu, Y. Cao, *Macromolecules (Washington, DC, USA)* **2010**, *43*, 9771–9778.

[15] a) Z. Ning, H. Tian, *Chem. Commun.* **2009**, 5483–5495; b) A. Mishra, M. K. R. Fischer, P. Bäuerle, *Angew. Chem.* **2009**, *121*, 2510; *Angew. Chem. Int. Ed.* **2009**, *48*, 2474–2499; c) A. Hagfeldt, G. Boschloo, L. Sun, L. Kloo, H. Pettersson, *Chem. Rev.* **2010**, *110*, 6595–6663.

[16] D. N. Lee, J. K. Kim, H. S. Park, Y. M. Jun, R. Y. Hwang, W.-Y. Lee, B. H. Kim, *Synth. Met.* **2005**, *150*, 93–100.

[17] a) Y. Nishikitani, T. Kubo, H. Masuda, *Mol. Cryst. Liq. Cryst.* **2011**, *538*, 1–9; b) Z. Jin, H. Masuda, N. Yamanaka, M. Minami, T. Nakamura, Y. Nishikitani, *ChemSusChem* **2008**, *1*, 901–904.

[18] D. Cież, J. Svetlik, *Synlett* **2011**, 315–318.

[19] E. Täuscher, D. Weiß, R. Beckert, H. Görls, *Synthesis* **2010**, 1603–1608.
[20] a) B. P. Fors, P. Krattiger, E. Strieter, S. L. Buchwald, *Org. Lett.* **2008**, *10*, 3505–3508; b) D. S. Surry, S. L. Buchwald, *Angew. Chem.* **2008**, *120*, 6438; *Angew. Chem. Int. Ed.* **2008**, *47*, 6338–6361.
[21] A. Sakalyte, J. Simokaitiene, A. Tomkeviciene, J. Keruckas, G. Buika, J. V. Grazulevicius, V. Jankauskas, C.-P. Hsu, C.-H. Yang, *J. Phys. Chem. C* **2011**, *115*, 4856–4862.
[22] a) S. Thayumanavan, S. Barlow, S. R. Marder, *Chem. Mater.* **1997**, *9*, 3231–3235; b) P. Zacharias, M. C. Gather, M. Rojahn, O. Nuyken, K. Meerholz, *Angew. Chem.* **2007**, *119*, 4467; *Angew. Chem. Int. Ed.* **2007**, *46*, 4388–4392.
[23] M. R. Biscoe, T. E. Barder, S. L. Buchwald, *Angew. Chem.* **2007**, *119*, 7370; *Angew. Chem. Int. Ed.* **2007**, *46*, 7232–7235.
[24] a) O. Johansson, *Synthesis* **2006**, 2585–2589; b) R. A. Altman, S. L. Buchwald, *Nat. Protocols* **2007**, *2*, 3115–3121.
[25] X. Wu, A. P. Davis, P. C. Lambert, L. Kraig Steffen, O. Toy, A. J. Fry, *Tetrahedron* **2009**, *65*, 2408–2414.
[26] a) A. N. Sobolev, V. K. Belsky, I. P. Romm, N. Y. Chernikova, E. N. Guryanova, *Acta Crystallogr., Sect. C* **1985**, *41*, 967–971; b) E. Täuscher, L. Calderón-Ortiz, D. Weiß, R. Beckert, H. Görls, *Synthesis* **2011**, 2334–2339.
[27] a) J. McDowell, *Acta Crystallogr., Sect. B* **1976**, *32*, 5–10; b) C. L. Klein, J. M. Conrad III, S. A. Morris, *Acta Crystallogr., Sect. C* **1985**, *41*, 1202–1204.
[28] a) M. V. Jovanovic, E. R. Biehl, R. D. Rosenstein, S. S. C. Chu, *J. Heterocycl. Chem.* **1984**, *21*, 661–667; b) J. R. Huber, W. W. Mantulin, *J. Am. Chem. Soc.* **1972**, *94*, 3755–3760.
[29] X. Zhang, Z. Chi, Z. Yang, M. Chen, B. Xu, L. Zhou, C. Wang, Y. Zhang, S. Liu, J. Xu, *Opt. Mater.* **2009**, *32*, 94–98.
[30] a) J. M. Chudomel, B. Yang, M. D. Barnes, M. Achermann, J. T. Mague, P. M. Lahti, *J. Phys. Chem. A* **2011**, *115*, 8361–8368; b) R. Hu, E. Lager, A. l. Aguilar-Aguilar, J. Liu, J. W. Y. Lam, H. H. Y. Sung, I. D. Williams, Y. Zhong, K. S. Wong, E. Pena-Cabrera, B. Z. Tang, *J. Phys. Chem. C* **2009**, *113*, 15845–15853; c) H. Cao, V. Chang, R. Hernandez, M. D. Heagy, *J. Org. Chem.* **2005**, *70*, 4929–4934; d) K. Rotkiewicz, K. H. Grellmann, Z. R. Grabowski, *Chem. Phys. Lett.* **1973**, *19*, 315–318.
[31] N. Asami, T. Takaya, S. Yabumoto, S. Shigeto, H.-o. Hamaguchi, K. Iwata, *J. Phys. Chem. A* **2010**, *114*, 6351–6355.
[32] a) J. R. Lakowicz, *Principles of fluorescence spectroscopy*, 3rd ed., Springer, New York, **2006**; b) N. Mataga, Y. Kaifu, M. Koizumi, *Bull. Chem. Soc. Jpn.* **1955**, *28*, 690–691.
[33] E. Lippert, *Z. Naturforsch., A* **1955**, *10*, 541–545.
[34] E. Lippert, *Z. Elektrochem. Ber. Bunsenges. Physik. Chem.* **1957**, *61*, 962–975.
[35] a) S. Techert, K. A. Zachariasse, *J. Am. Chem. Soc.* **2004**, *126*, 5593–5600; b) E. Castanheira, A. Abreu, M. Carvalho, M.-J. Queiroz, P. Ferreira, *J. Fluoresc.* **2009**, *19*, 501–509; c) Z. R. Grabowski, K. Rotkiewicz, W. Rettig, *Chem. Rev.* **2003**, *103*, 3899–4032; d) K. Rurack, in *Standardization and Quality Assurance in Fluorescence Measurements I*, vol. 5 (Ed.: U. Resch-Genger), Springer, Berlin, Heidelberg, **2008**, pp. 101–145.
[36] B. Happ, D. Escudero, M. D. Hager, C. Friebe, A. Winter, H. Gorls, E. Altuntas, L. González, U. S. Schubert, *J. Org. Chem.* **2010**, *75*, 4025–4038.
[37] J. L. Zambrana, E. X. Ferloni, J. C. Colis, H. D. Gafney, *Inorg. Chem.* **2007**, *46*, 2–4.
[38] E. C. Glazer, D. Magde, Y. Tor, *J. Am. Chem. Soc.* **2007**, *129*, 8544–8551.
[39] E. C. Glazer, D. Magde, Y. Tor, *J. Am. Chem. Soc.* **2005**, *127*, 4190–4192.
[40] X.-y. Wang, A. Del Guerzo, R. H. Schmehl, *J. Photochem. Photobiol. C: Photochem. Rev.* **2004**, *5*, 55–77.
[41] E. Runge, E. K. U. Gross, *Phys. Rev. Lett.* **1984**, *52*, 997–1000.
[42] J. Tomasi, B. Mennucci, R. Cammi, *Chem. Rev.* **2005**, *105*, 2999–3094.
[43] M. J. Frisch, G. W. Trucks, H. B. Schlegel, G. E. Scuseria, M. A. Robb, J. R. Cheeseman, G. Scalmani, V. Barone, B. Mennucci, G. A. Petersson, H. Nakatsuji, M. Caricato, X. Li, H. P. Hratchian, A. F. Izmaylov, J. Bloino, G. Zheng, J. L. Sonnenberg, M. Hada, M. Ehara, K. Toyota, R. Fukuda, J. Hasegawa, M. Ishida, T. Nakajima, Y. Honda, O. Kitao, H. Nakai, T. Vreven, J. A. Montgomery, J. E. Peralta, F. Ogliaro, M. Bearpark, J. J. Heyd, E. Brothers, K. N. Kudin, V. N. Staroverov, R. Kobayashi, J. Normand, K. Raghavachari, A. Rendell, J. C. Burant, S. S. Iyengar, J. Tomasi, M. Cossi, N. Rega, J. M. Millam, M. Klene, J. E. Knox, J. B. Cross, V. Bakken, C. Adamo, J. Jaramillo, R. Gomperts, R. E. Stratmann, O. Yazyev, A. J. Austin, R. Cammi, C. Pomelli, J. W. Ochterski, R. L. Martin, K. Morokuma, V. G. Zakrzewski, G. A. Voth, P. Salvador, J. J. Dannenberg, S. Dapprich, A. D. Daniels, O. Farkas, J. B. Foresman, J. V. Ortiz, J. Cioslowski, D. J. Fox, *Gaussian 09*, rev. B.01, Gaussian, Inc., Wallingford CT, **2009**.
[44] a) A. D. Becke, *J. Chem. Phys.* **1993**, *98*, 5648–5652; b) C. Lee, W. Yang, R. G. Parr, *Phys. Rev. B* **1988**, *37*, 785–789.
[45] J. Guthmuller, B. Champagne, *J. Chem. Phys.* **2007**, *127*.
[46] A. D. Becke, *Phys. Rev. A* **1988**, *38*, 3098–3100.
[47] P. C. Hariharan, J. A. Pople, *Theor. Chim. Acta* **1973**, *28*, 213–222.
[48] a) W. Schmidt, E. Steckhan, *Chem. Ber.* **1980**, *113*, 577–585; b) M. Matis, P. Rapta, V. R. Lukes, H. Hartmann, L. Dunsch, *J. Phys. Chem. B* **2010**, *114*, 4451–4460; c) L. Hagopian, G. Koehler, R. I. Walter, *J. Phys. Chem.* **1967**, *71*, 2290–2296.
[49] O. Yurchenko, D. Freytag, L. zur Borg, R. Zentel, J. Heinze, S. Ludwigs, *J. Phys. Chem. B* **2011**, *116*, 30–39.
[50] V. Dvořák, I. Němec, J. Zýka, *Microchem. J.* **1967**, *12*, 350–370.
[51] J. F. Ambrose, L. L. Carpenter, R. F. Nelson, *J. Electrochem. Soc.* **1975**, *122*, 876–894.
[52] S. M. Bonesi, R. Erra-Balsells, *J. Lumin.* **2001**, *93*, 51–74.
[53] a) A. W. Franz, F. Rominger, T. J. J. Muller, *J. Org. Chem.* **2008**, *73*, 1795–1802; b) B. Paduszek, M. K. Kalinowski, *Electrochim. Acta* **1983**, *28*, 639–642; c) D. J. Freed, L. R. Faulkner, *J. Am. Chem. Soc.* **1972**, *94*, 4790–4792.
[54] Y. Zhu, A. P. Kulkarni, S. A. Jenekhe, *Chem. Mater.* **2005**, *17*, 5225–5227.
[55] X.-Q. Zhu, Z. Dai, A. Yu, S. Wu, J.-P. Cheng, *J. Phys. Chem. B* **2008**, *112*, 11694–11707.
[56] P. J. Elving, J. E. O'Reilly, *J. Am. Chem. Soc.* **1971**, *93*, 1871–1879.
[57] J. E. O'Reilly, P. J. Elving, *J. Am. Chem. Soc.* **1972**, *94*, 7941–7949.
[58] a) M. R. McDevitt, A. W. Addison, *Inorg. Chim. Acta* **1993**, *204*, 141–146; b) C. M. Elliott, E. J. Hershenhart, *J. Am. Chem. Soc.* **1982**, *104*, 7519–7526.
[59] J. Pommerehne, H. Vestweber, W. Guss, R. F. Mahrt, H. Bässler, M. Porsch, J. Daub, *Adv. Mater.* **1995**, *7*, 551–554.
[60] S. Rau, M. Ruben, T. Buttner, C. Temme, S. Dautz, H. Görls, M. Rudolph, D. Walther, A. Brodkorb, M. Duati, C. O'Connor, J. G. Vos, *J. Chem. Soc., Dalton Trans.* **2000**, 3649–3657.
[61] a) R. Hooft, Nonius BV, Delft, The Netherlands, **1998**; b) Z. Otwinowski, W. Minor, in: *Methods Enzymol.*, vol. 276 (Ed.: Charles W. Carter Jr,), Academic Press, **1997**, pp. 307–326.
[62] G. Sheldrick, *Acta Crystallogr., Sect. A* **2008**, *64*, 112–122.

Received: May 22, 2012
Published Online: ■

Donor–Acceptor Dyes

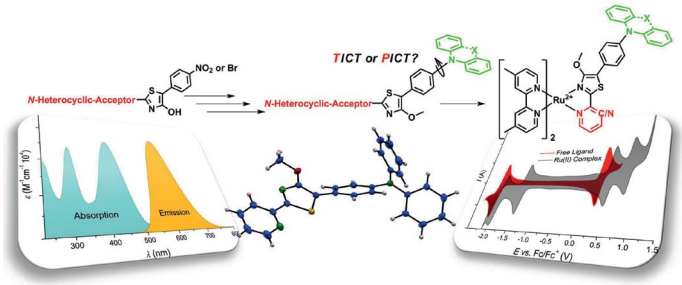

Several 4-hydroxy-1,3-thiazole-based chromophores bearing different arylamine donor and N-heterocyclic acceptor moieties were synthesized and their electronic properties were investigated experimentally and theoretically (DFT and TDDFT). The nature of the charge-transfer transition was identified. Additionally, the dyes were applied as light-harvesting ligands in heteroleptic Ru^{II} complexes.

Keywords: N,S-Heterocycles / Heterocycles / Chromophores / Dyes / Charge transfer / Density functional calculations / Ruthenium complexes

